Seismic Anisotropy and Its Geodynamic Implications in Iran, the Easternmost Part of the Tethyan Belt

Amir Sadeghi-Bagherabadi[1,2,3], Lucia Margheriti[2], Abdelkrim Aoudia[3], and Farhad Sobouti[1]

[1]Department of Earth Sciences, Institute for Advanced Studies in Basic Sciences (IASBS), Zanjan, Iran.

[2]Istituto Nazionale di Geofisica e Vulcanologia, Rome, Italy.

[3]Earth System Physics Section, Abdus Salam International Centre for Theoretical Physics, Trieste, Italy.

Corresponding author: Amir Sadeghi-Bagherabadi (Amir.Sadeghi@Hotmail.com)

Key Points:

- Anisotropic structure of the upper mantle in western Iran is studied through SKS splitting measurements.
- The dominant source layers of anisotropy in different tectonic blocks of the collision zone have been determined.
- Inferences on the organization of the sub-lithospheric flow field under the collision zone have been made.

This article has been accepted for publication and undergone full peer review but has not been through the copyediting, typesetting, pagination and proofreading process which may lead to differences between this version and the Version of Record. Please cite this article as doi: 10.1029/2018TC005209

Abstract

In this study, we use the results of seismic anisotropy as inferred from shear wave splitting analyses of SKS phases to propose a geodynamical model of the Arabia-Eurasia collision zone. A detailed analysis of the 202 non-null splitting and 196 null splitting measurements obtained from a dense temporary network are utilized to investigate the possibility of lateral and vertical variations in the anisotropic parameters and the hypothesis of a dipping anisotropic layer. A 2D geodynamical model of the western part of the collision zone is constructed. The preferred 2D model suggests that the belt-parallel orientation of fast axes in the western Zagros originates from a lithospheric transpressional deformation. The plate motion-parallel pattern in central Iran and western Alborz coincides with the decrease in the lithospheric thickness. Thus, we believe this trend has its origin in the asthenosphere. A combination of the keel effect of the thickened Zagros lithosphere, the asthenospheric edge-driven convection flow and the lithospheric deformation in the shear zones can cause the NW-SE oriented splitting pattern reported in some parts of central Iran. The asthenospheric flow beneath the thinner lithosphere to the south of the Bitlis suture in northern Iraq is likely the causative mechanism for our observed plate motion-parallel splittings there. The variation of the convergence obliquity along the Alborz and Zagros inferred from analysis of geodetic data implies that a change in the pattern of lithospheric deformation and the consequent anisotropy is expected.

1 Introduction

There are various methods to investigate the seismic anisotropy of the upper mantle, amongst them, the splitting analysis of the core refracted shear wave phases is one of the most commonly used. Linking the anisotropic structure with the strain fabric of the deforming medium under the seismic stations is the ultimate goal of shear wave splitting analysis. Lattice Preferred Orientation (LPO) of anisotropic minerals and Shape Preferred Orientation (SPO) of aligned cracks are two principal mechanisms for shear wave splitting. In the oceanic regions, the general global agreement between the observed uniform seismic anisotropy with the plate motion vectors implies that anisotropy in the oceans originates from the asthenospheric flow field. In the continents, anisotropic patterns are much more complicated and vary on short spatial scales (Long and Becker, 2010). Considering the fact that the continents have thicker lithosphere in comparison with the oceans, significant contribution from the continental mantle lithosphere to shear wave splitting is expected. Shear wave splitting observations in convergent margins have some of the most complicated patterns. In subduction and collision zones, more often than not both the lithospheric deformation and the asthenospheric flow field contribute to the observed anisotropy.

The subduction of the Paleo-Tethys and the Neo-Tethys ocean basins under Eurasia and the subsequent collision of Arabia with Eurasia over a very long geological time span have resulted in the formation of a geodynamic assemblage in the Iran region composed of the Zagros, Alborz and Kopet Dagh fold-and-thrust belts, the Sanandaj-Sirjan (SSZ) and Urmieh-Dhokhtar (UDMA) magmatic arcs, and the central and eastern Iran micro-continental blocks (Figure 1). The Zagros collision started in the Oligocene. It first affected the SSZ, and progressively moved south to the High Zagros during the Miocene, and since the Pliocene it has reached its peak in the Fold-and-Thrust Belt (Alavi, 1994; Agard et al., 2011; Mouthereau et al., 2012). The SSZ and UDMA Neo-Tethyan volcanic arc structures developed during the Mesozoic and the Cenozoic, respectively, as the dynamics of the subduction zone changed during the course of time (Agard et al., 2011). The Arabia-Eurasia collision zone is a natural laboratory for the study of the geodynamics of the continental

collision and lithospheric/asthenospheric deformation during the early stages of mountain building.

There has been a limited number of studies on seismic anisotropy in the Arabia-Eurasia collision zone, and in particular in the Iranian plateau. The first major study was by Kaviani et al. (2009). They used the shear wave splitting of the core refracted phases and reported a complicated pattern composed of null measurements in the main mountain belts (i.e. Zagros, Alborz and Kopet Dagh), and a predominantly NW-SE trend of fast-axes in central Iran that rotates to a NE-SW direction in northeast Iran. Sadidkhouy et al. (2008) studied mantle anisotropy in central Alborz and observed a NE-SW directed anisotropy at stations very close to the NW-SE trending and/or null observations of Kaviani et al. (2009). Studies by Arvin et al. (2014) in NW Iran and Moradi et al. (2015) in western Alborz also showed a dominant NE-SW trend of the fast-axes. Sadeghi-Bagherabadi et al. (2018) reported non-null station average measurements with fast-axes subparallel to the trend of the mountain range in the Zagros (NW-SE) (Figure 1). In the Alborz they obtained NE-SW directed fast-axes at a sharp angle to the strike of the mountains there, in accordance with the works of Sadidkhouy et al. (2008), Arvin et al. (2014), and Moradi et al. (2015). Sadeghi-Bagherabadi et al. (2018) proposed that both the lithospheric and the asthenospheric mantle contribute to the SKS splitting observations in Iran and the relative contribution of each layer in a given region is determined by the thickness of the lithosphere. Moreover, results of several studies on Pn velocity structure (Al-Lazki et al., 2014; Lü et al., 2012) including a recent anisotropic Pn tomography with Moho depth correction (Lü et al., 2017) provide valuable clues to define the lithospheric anisotropy in the region.

Most of the above-mentioned studies agree that in Iran the values of the average delay times between the fast and slow birefringent waves, are about 1 sec throughout the region and do not show significant variations. On the other hand, the average fast polarization orientations dramatically vary when crossing from one tectonic block into another. In this paper we expand on the work of Sadeghi-Bagherabadi et al. (2018) by presenting the entire set of individual measurements, detecting and analyzing the variations in the measurements, and investigating the origin and source layers of the observed anisotropic domains. We also speculate about the reasons for the changes in the fast polarization orientations across the collision zone. By combining the results of our analysis with the current state of knowledge of the geometry and deep structure of the lithosphere and the upper mantle of Iran, we aim to develop a model that can improve our understanding of the geodynamic evolution of the Arabia-Eurasia convergence zone.

2 Methods and Results

Our data came from a temporary network of 63 broadband stations covering the entire collision zone in western Iran that was in operation for one year in 2013-2014 (see Figure 1) (Sadeghi-Bagherabadi et al., 2018). The small station spacing (about 13 km) allowed for the detection of a complex anisotropic pattern. A similar situation was analyzed in the Alps by Salimbeni et al. (2018). Records of teleseismic earthquakes with $M \geq 6.0$ in the epicentral distance range between 90° and 130° are examined to analyze the SKS/SKKS phases using SplitLab software (Wüstefeld et al., 2008). The minimum energy method of Silver and Chan (1991) is adopted. This method estimates the splitting parameters by minimizing the energy on the transverse component through a grid search over all possible pairs of fast-axis orientations (φ) and delay times (δt). The seismograms are band-pass filtered between 0.04 and 0.25 Hz in order to maximize the signal-to-noise ratio.

A total number of 202 non-null splitting parameters and 196 null measurements were obtained (Table S1). We considered a delay time threshold of 0.5 sec as a reliable non-null measurement. There were only 14 individual measurements with delay time larger than 2 sec and the largest value was 3.5 sec measured at station W06 in central Iran. We observed variations of the results at some stations that lead us to focus on the individual measurements in order to gain a better understanding of the origin of the anisotropy.

Figure 2 shows the single measurements along the three profiles of the seismic network. Measurements are plotted as cyan segments scaled with their respective delay time above their ray piercing point at the depth of 150 km. This way of visualization better positions the single measurements in the probable anisotropic volume they sample. The two best-recorded earthquakes with back-azimuths of 290° and 85° had 26 and 21 non-null splitting measurements, respectively. The results obtained from these two events show sharp variations of fast orientation along the profiles. Along the southern part of the transects in the Zagros mountains, events with incoming rays from the east yielded about 35 good-quality results with the fast-axes mostly oriented NW-SE. Events from the west, on the other hand, returned mainly null measurements (~50 measurements). In the Alborz mountains, in the north of the investigated area, the fast orientations of about 60 non-null measurements are consistently NE-SW and coherent from all available back-azimuths. In the central parts of the transect which coincide with the central Iran region, we obtained about 75 non-null measurements with variable fast-axis orientations.

2.1 Lateral Variations of Anisotropy

The observed variations of fast orientations described in the previous section can originate from lateral changes in the anisotropic structures. We investigated the changes in the splitting results of seven events with similar back-azimuths (84° to 91°) to verify the consistency of the results between the different events and to detail the lateral variations in the anisotropic pattern across the transect. Abrupt changes in the fast orientations were observed for these seven events (Figure 3). The main changes in the fast orientations occur in the regions between Zagros, Central Iran and Alborz. We also examined in detail the splitting parameters of two well-recorded earthquakes coming from opposite back-azimuths (290° and 300°), as well as one event from the south (back-azimuth 200°). In Figure 3a and 3b the individual measurements of earthquakes with similar back-azimuths are plotted together. The best-recorded events are shown by brown triangles, and the rest of the measurements by circles. This analysis, highlights an important variability in the fast-axis behavior, in particular in the Zagros and central Iran where the fast-axis orientations obtained from rays coming from the east (back-azimuths smaller than 180°) are different from those coming from the west (back-azimuths greater than 180°). The Alborz stations are an exception to this trend for which all of the SKS waves, regardless of their back-azimuth, give fast-axes in the NE-SW direction, subparallel to the absolute plate motion direction. In Figure 3c and 3d we have highlighted this variability by dividing the results into two groups (back-azimuths smaller and greater than 180°) and projecting them along the profile. The single measurements obtained in Alborz are shown by green diamonds and those of Zagros and central Iran (which are back-azimuth dependent) are illustrated by inverted purple triangles. Frequency rose diagrams of the two groups are plotted in Figure 3e and 3f. In the Zagros and central Iran regions, the rose diagram (purple colored) for the eastern events shows a SE-NW trend which is parallel to the Zagros strike (Figure 3f). The western rays, on the other hand, returned many nulls measurements (Figure 2), but the remaining non-null measurements show fast orientations with a SW-NE trend (Figure 3e). We computed the average of fast-axis orientations for the eastern and western back-azimuths, separately. The average fast-axes

calculated for the Alborz and those outside Alborz (Zagros and central Iran) are shown by green and purple bars in Figure 3c and 3d, and by green diamonds and purple triangles in Figure 3e and 3f, respectively. The directional statistics (Davis, 1986; Mardia and Jupp, 2000) is commonly used for calculation of the average fast polarization orientation. Here we utilized the bidirectional circular average (Liu and Gao, 2011; Gao and Liu, 2012; Sadeghi-Bagherabadi et al., 2018) (Figure S1):

$$\bar{\varphi} = \begin{cases} 0.5\, tan^{-1}\left(S/C\right), S \geq 0, C \geq 0 \\ 0.5\left(tan^{-1}\left(S/C\right) + 180°\right), C < 0 \\ 0.5\left(tan^{-1}\left(S/C\right) + 360°\right), S < 0, C > 0 \end{cases} \quad (1)$$

where $S = 1/N \sum_{i=1}^{N} sin(2\varphi_i)$ and $C = 1/N \sum_{i=1}^{N} cos(2\varphi_i)$, φ_i is the *i*th measured fast orientation and *N* is the number of measurements at the station.

Due to near-vertical incidence of the core-refracted phases at the surface, seismic anisotropy of the upper mantle as inferred from shear wave splitting has a very good lateral resolution in comparison with other techniques (e.g. anisotropic surface wave tomography). On the other hand, since shear wave splitting is an integrated effect through a traveling path, it has an inferior vertical resolution compared to surface wave tomography. The ray paths of the core-refracted phases diverge from the vertical with increase in depth, and the size of the first Fresnel zone which is an approximation for the sampled volume at depth grows in size for deeper piercing depths and longer periods. The radius of the first Fresnel zone can be approximated by $(TVD/2\cos\theta)^{0.5}$, where T is the dominant period, V is the wave velocity, D is the depth of interest, and θ is the incidence angle. These geometrical features of the ray paths can be utilized to put depth constraints on the lateral changes of anisotropy measured at the surface (e.g. Alsina and Snieder, 1995; Margheriti et al., 2003; Salimbeni et al., 2008). We used two earthquakes with opposite back-azimuths with differing splitting parameters measured at the same station to estimate the upper depth limit of the causative anisotropic lateral gradient. We found good couple of measurements for this analysis at stations E01, M01, M04 and M06 (Figure 4a). In order to constrain the top of the anisotropic source layer, we assumed a 10% overlap between the Fresnel zones of the two opposing ray paths with differing splitting results as a requirement to distinguish two separate regions at depth. The results of the analysis are shown in Figure S2. According to the results the depth of the anisotropic volume should be greater than 200 km beneath stations M01 and E01 near the southwestern margins of the Zagros range and it should increase to more than 250 km under stations M04 and M06 in the interior of the Zagros. Another earthquake pair with opposite back-azimuths and dissimilar splitting parameters measured at station M27 in central Iran gave a very different depth range. There, the analysis implies that the anisotropic layer could be as shallow as 140 km (Figure 4a and Figure S2).

Since the station spacing on the main profile is small (~13 km) a similar procedure can be applied to pairs of nearby stations with dissimilar splitting measurements from the same event in order to estimate the bottom limit of the anisotropic layer. To make sure that the anisotropic change occurs along the line of the ray paths, this analysis should be preferably done with events coming from azimuths parallel to the stations alignment. In the absence of such well-recorded earthquakes, we used events with back-azimuths non-parallel to the stations alignment. Although, this would not result in very rigorous estimation of bottom limit of the anisotropic source layer, it still can provide clues as to how the depth of anisotropic layer changes along the profile. We estimated the overlap areas of the first Fresnel zones at depths of 50 to 350 km from one event with back-azimuth 291° recorded at stations M19 and M22, and two events with back-azimuth 90° recorded at stations M31 and

M37, and stations M01 and M04 (Figure 4b). Different radii of the Fresnel zones in Figure 4 at M31 and M37 are because of the slight difference in the periods of the analyzed seismic phases. The results suggest that the anisotropic layer could be as shallow as about 50 km beneath M01, M04, M19 and M22, all of them in the Zagros region and the SSZ (Figure 4b, Figure S2). In central Iran the result of the analysis at stations M31 and M37 shows that the depth of the anisotropic gradient should be approximately less than 150 km (Figure 4b, Figure S2).

The rough estimate of very shallow 50-km anisotropic gradient in the Zagros is not in agreement with the 200-to-250-km top-of-the-layer estimates in the same region. Considering the average delay time of 1.4 sec in the Zagros, if anisotropy were confined in the upper 50 km it would require an unusually-high 10% vertically-coherent crustal anisotropy. Moreover, in other orogenic belts such as the Alps, Tibet and Taiwan, layered lithospheric anisotropy has been reported (Ozacar and Zandt, 2004; Fry et al., 2010; Huang et al., 2015), which is irreconcilable with the assumption of vertically-coherent anisotropy. On the other hand, the deep origin of anisotropy (asthenospheric) inferred from the Fresnel zones under E01, M01, M04, and M06 in the Zagros may not also necessarily account for the observed average delay times because it depends on the depth of the transition from dislocation creep to diffusion creep (Mainprice et al., 2005). A potential explanation could be that the observed delay times do not originate from a single anisotropic layer, but are rather an aggregated response from multiple anisotropic volumes.

2.2 Multi-Layer Anisotropy with Perpendicular Fast-axes

The back-azimuthal dependency of the splitting parameters at the surface can be considered as an indicator of a complex anisotropic structure at depth. The two-layer anisotropy with horizontal symmetry axes exhibits periodicity as a function of incoming polarization in the observed splitting measurements at the stations (apparent splitting parameters). The back-azimuthal coverage of the recorded events at stations is not sufficient to model this kind of structure. Nevertheless, the observations gave us an idea about a special case of two-layer anisotropy with perpendicular fast-axes. This particular configuration does not show the periodicity and is not easily distinguishable from a single layer anisotropy with horizontal symmetry axis. In this case, the fast-axis orientation of one layer is parallel to the slow orientation in the other layer. The incoming wave will be polarized and split in the lower layer, and the effect of the upper layer will be to reduce the delay time produced in the lower layer. The apparent fast orientation will be parallel to the fast orientation of the thicker layer or to that of the layer with stronger anisotropy. The apparent delay time will be the sum of the positive delay time in the dominant layer and the negative time lag produced by the other layer. Figure S3 shows this setting; equal strength of anisotropy in both layers will lead to an apparent null observation.

Our measurements show two main perpendicular patterns of anisotropy along the profile (Figure 2 and 3). The mountain-parallel trend in the Zagros might be a result of deformation in the thick lithosphere of the Arabian plate and the mountain-perpendicular trend in the Alborz which is subparallel to the GPS velocity vectors in the no-net-rotation (NNR) reference frame could originate from the sub-lithospheric (asthenospheric) flow (Sadeghi-Bagherabadi et al., 2018). In central Iran region, two abrupt changes in the fast polarization orientations are evident along the profiles: the first one is the change from mountain-parallel trend in the Zagros to mountain strike-perpendicular (plate motion-subparallel) in the SSZ and central Iran, and the second change is further north where a sharp rotation to range-parallel trend occurs inside the central Iran major shear zones (Figure 2). The latter mountain range-parallel fast orientations in central Iran were also observed by

Kaviani et al. (2009) and they interpreted this trend as a result of the vertically-coherent deformation of the lithosphere.

The interpretations provided by the previous studies in the region lead to the conclusion that the mountain-range parallel and perpendicular trends in fast orientations might have lithospheric and sub-lithospheric origins, respectively (Sadeghi-Bagherabadi et al., 2018). Based on this hypothesis, we constructed, for each station, a simple two-layer model of orthogonal fast axes, with the lower layer having a fast orientation of 45^{o} (range-perpendicular), and the upper layer a fast orientation of 135° (range-parallel). We simplified the observed fast-axis orientation of the station by replacing it with the fast-axis of one of the model layers (45° or 135°), whichever was closer. The delay time of each layer was chosen such that the algebraic sum of the two delay times would be equal to the observed apparent delay time of the station. This gave us a set of models all having the same apparent delay time but a range of layer delay times (see Figure S4). In our modelling, the delay time of the layer with fast-axis perpendicular to the simplified observation was allowed to vary from 0 (isotropic) to 1 sec. We smoothed the trend of the delay times in the layers along the profile (Figure 5c and 5d). The trend of the delay times was converted to thickness (Figure 5e) using a nominal 4% global anisotropy in the upper mantle (Savage, 1999). Assuming that the upper and lower layers represent the anisotropic lithosphere and asthenosphere, respectively, the trade-off between their thicknesses can be used to infer an estimate of the depth of the Lithosphere-Asthenosphere Boundary (LAB) and the maximum anisotropic depth of the asthenosphere (Mainprice et al., 2005). Regardless of the absolute LAB depths estimated for different delay time models, a similar pattern of the lithospheric thickness variation along the profile is obtained. We observe shallow LAB to the north of the SSZ and deeper LAB beneath the Zagros and central Iran. This model gives clues for a thin lithosphere under the Alborz and a thicker one under the Zagros. A comparison between the absolute LAB depths in Figure 5e and the lithospheric thickness obtained by other geophysical studies can help to select the best-fitting model.

2.3 A Dipping Anisotropic Layer

In the previous sections we discussed the variation of splitting parameters with opposing back-azimuths in a single station as indicator of lateral or vertical anisotropic gradient. This observation can also be interpreted as indicator of back-azimuthal dependency with 2π periodicity caused by a dipping anisotropic layer. The splitting parameters of stations M01 and E01 show such variation with back-azimuth. We utilized this observation to examine whether a dipping anisotropic layer is present under these stations. For the purpose of this modeling we used the MSAT toolkit (Walker and Wookey, 2012). MSAT uses the single-crystal elasticity information of olivine by Abramson et al., (1997) and calculates the Voigt-Reuss-Hill average elasticity of the aggregated minerals (Hill, 1952; Walker and Wookey, 2012). It then estimates the phase velocities and splitting parameters by solving the Christoffel equation (Crosson and Lin, 1971; Mainprice, 1990; Walker and Wookey, 2012).

There are too many unknown parameters to be estimated for constructing a dipping anisotropic layer model, such as the orientation, dip, and thickness of the layer, as well as the fast-axis azimuth of the layer. Attempting to estimate all of them simultaneously, using our data, would not give reliable results. Therefore, we first fixed the thickness of the anisotropic layer and the azimuth of the horizontal projection of the dip vector at 250 km and 45°, respectively. The 45° dip vector was chosen so as to be perpendicular to the strike of the Zagros. The principal influence of the layer thickness is on the delay time, while the back-azimuthal dependency of the fast polarization orientation remains insensitive to it. The volume fraction of crystal alignment also affects the absolute values of the delay times. We

performed a grid search over pairs of dip angles (ranging from 0°, horizontal, to 90°, vertical) and fast-axis azimuths (ranging from 0° to 180°) to find the best model that minimizes the summation of the Chi-squares of fast orientation and delay time (Margheriti et al., 2003; Walker et al., 2005; Fontaine et al., 2007; Salimbeni et al., 2013; Qorbani et al., 2015). Existence of a very wide back-azimuthal gap (between 90° and 270°) in our dataset led to a non-uniqueness in the final model (Figure S5). Despite this, a steeply NE-dipping model with dip angle of 77° and fast-axis azimuth of 61° best fits the observations (Figure S5). We repeated the same procedure for different azimuths of the horizontal projection of the dip vector and the best-fitting model was a 76° dipping layer with layer strike of 50° and fast-axis azimuth 58°. This model is not significantly different from the result obtained by fitting the fixed orientation model (Figure S6).

3 Discussions

3.1 Potential Geodynamic Scenarios Describing the Shear Wave Splitting Observations

The complicated pattern of shear wave splitting observations in the Arabia-Eurasia collision zone is the result of the ongoing and past geodynamic and tectonic processes in the region. The main current structural features of the Iranian region are the three orogenic belts of Zagros, Alborz and Kopet Dagh, the volcanic arcs of SSZ and UDMA, and the central Iran micro-continent. The past subductions of the Paleo-Tethys and the Neo-Tethys had key roles in the formation of the deep structure of the Iranian plateau and still influences the geodynamics of the region. The ages for the closure of the Neo-Tethys and the onset of continental collision remains controversial and the published ages vary from more than 40 Ma to less than 10 Ma (Agard et al., 2011; Allen and Armstrong, 2008; Ballato et al., 2011; Dewey et al., 1973; Hempton, 1987; Khadivi et al., 2012; Saura et al., 2015; Stoneley, 1981; Talebian and Jackson, 2004; Zhang et al., 2016). As a result, the deformation history and the young orogeny in the Iranian plateau has been dominated by the subduction, as well as the collisional processes. On the one hand, the location and geometry of the dipping anisotropic layer presented in section 2.3 supports the idea of the presence of a steep slab inherited from the past ocean-continent convergence. On the other hand, the lithospheric structure reconstructed from the multi-layer anisotropic model in section 2.2 is more oriented to a lithospheric structure shaped up by the more recent continent-continent collisional process. In the following we will discuss each of the main structural features that have been sampled by our splitting measurements.

3.1.1 The Zagros

Shear wave splitting fast-axes, parallel or subparallel to the strike of the convergent borders either in the active subduction zones or continental collisions, have been reported in many regions of the world. Toroidal mantle flow at slab edge (Civello and Margheriti, 2004; Zandt and Humphreys, 2008; Faccenda and Capitanio, 2012), tilted radial anisotropy beneath the steep slabs (Song and Kawakatsu, 2012; Song and Kawakatsu, 2013), and the tilted transverse isotropy with a slow symmetry axis pointing normal to the plane of the slab (Walpole et al., 2017) are the main proposed explanations for the observed trench-parallel trends in subduction zones. The mountain chain-subparallel trend similar to the pattern we have reported in the Zagros has also been observed in many other mountain chains (Silver, 1996; Meissner et al., 2002; Barruol et al., 2011; Bokelmann et al., 2013). The asthenospheric flow (Margheriti et al., 1996; Baccheschi et al., 2007; Barruol et al., 2011) or deformation in the continental crust above the slab (Wölbern et al., 2014) in subduction-associated mountains, transpressional deformation of the lithosphere (Silver and Chan, 1991; Nicolas,

1993; Silver, 1996), and lithospheric extrusion in response to the mountain-perpendicular stresses (Meissner et al., 2002) are the main mechanisms for the chain subparallel fast-axis orientation in mountain ranges.

In central Zagros a slab retreat is believed to have happened after the onset of the collision in late Oligocene that was followed by a slab break-off after late Miocene (Hafkenscheid et al., 2006; Agard et al., 2011). Formation of adakites in central Zagros has been proposed as evidence for the slab break-off (Omrani et al., 2008; Agard et al., 2011). However, because of lack of adakite magmatism in western Zagros and beneath our seismic profile, the fate of the Neo-Tethyan slab in this part of the Zagros is not clear. Considering different proposed mechanisms for the worldwide chain-parallel fast-axis orientations, there are two main geodynamic scenarios for explaining the mountain-subparallel trend in western Zagros depending on the situation of the Neo-Tethyan slab. A simplified 2D sketch depicting the two scenarios is presented in Figure 6.

In the case of a slab break-off under the Zagros, a transpressional deformation of the thickened lithosphere is a justifying scenario for the observed seismic anisotropy in western Zagros (Figure 6). If the slab has not been broken off and is still retreating, the asthenospheric lateral flow behind the slab can be an explanatory scenario for the trench-parallel fast-axis orientations (Figure 6b). A downward flow in response to the slab retreat can give rise to the dipping anisotropic layer discussed in section 2.3 (Figure S6). Since the Neo-Tethyan slab does not continue to the northwest and beneath the Bitlis suture, the asthenospheric toroidal flow around the slab can be considered as another justification for the trench-parallel pattern (Figure 6d). A crustal contribution to the anisotropy is always expected, but the probability that the splitting comes entirely from the crust is highly unlikely.

3.1.2 Central Iran

The slab retreat scenario proposed for the Zagros explains well the abrupt change from mountain chain-parallel to perpendicular orientation fast-axes in the north of SSZ. The south westward retreat of the subducting slab could have drawn, by suction, the asthenospheric material under central Iran towards the Zagros (similar mechanism was proposed for the Apennine-Tyrrhenian system by Barruol et al., 2011). This would result in a return flow that could justify the plate motion-subparallel observations to the north of the Zagros suture (Figure 6b). On the other hand, based on the slab break-off scenario, we can argue that to the north of SSZ the decrease in the lithospheric thickness coincides with the reduction in the transpressional deformation of the lithosphere. There, the lithosphere is thinner and less deformed, therefore, the observed anisotropy could originate from plate drag in the sub-lithosphere and result in the plate motion-parallel fast-axis orientations (Figure 6a).

The NW-SE fast-axis orientations in central Iran just to the south of the Alborz seem to be the continuation of the trend reported by Kaviani et al., (2009) in central Iran further southeast of our profile (Figure 1a). Kaviani et al. (2009) argued that this trend is aligned with the central Iran major shear zones and proposed that it reflects the lithospheric-scale of those shear zones. Priestley et al. (2012) interpreted the same NW-SE observations differently and suggested that the anisotropic source is located in the asthenosphere but that the thick Zagros lithospheric root distorts its surrounding asthenospheric flow field. An alternative justification for the NW-SE fast-axis orientations is based on the small-scale Edge-Driven Convective (EDC) flow (Kaislaniemi and Van Hunen, 2014; King and Anderson, 1998). EDC forms in the upper mantle at locations where significant discontinuities in the thickness of lithosphere exist. This lithospheric thickness gradient in turn, results in a horizontal temperature gradient that causes a convective flow. Kaislaniemi

and Van Hunen (2014) showed that EDC generates a significant edge-parallel horizontal flow component especially near the thickness gradients. In the slab break-off scenario, there is a lithospheric thickness gradient caused by the abrupt thinning of the lithosphere in central Iran (Mohammadi et al., 2013). This lithospheric thickness gradient beneath central Iran can give rise to the EDC with a NW-SE horizontal flow component parallel to the Zagros strike (Figure 6a).

Considering the individual splitting measurements, either the keel effect of the thickened lithosphere (i.e. the asthenospheric flow around the Zagros lithospheric root) (Figure 6c) or the toroidal flow around the western termination of the Neo-Tethyan slab (Figure 6d), are likely to account for the fast-axis variations in central Iran.

3.1.3 The Alborz

In the Alborz, plate motion-parallel (NE-SW) fast-axes were observed by Sadeghi-Bagherabadi et al. (2018) and Sadidkhouy et al. (2008). The same pattern has been reported by Arvin et al. (2014) in NW Iran and by Moradi et al. (2015) in western Alborz. In contrast, a NW-SE trend and a number of null stations were reported by Kaviani et al. (2009) in central Alborz (Figure 1). The same NE-SW trend is also observed by Sandvol et al. (2003) in eastern Turkey and in northeast Iran by Kaviani et al. (2009), implying that a large-scale asthenospheric flow can be a causative factor for the observed anisotropy (Figure 6).

3.2 Receiver Functions and Seismic Tomography versus the Proposed Geodynamic Scenarios

A comparison between the proposed geodynamic scenarios and our geophysical understanding of the deep structure of the region will help to gain a better picture about the most realistic scenario. Results of receiver function studies reveal some vital pieces of the geodynamic puzzle. Mohammadi et al. (2013) applied the S receiver function (SRF) method for mapping the Moho and LAB discontinuities in Iran and projected their migrated SRFs along three profiles perpendicular to the Strike of Zagros. The best image was obtained along their western profile which is very close to the seismic profiles used in this study. We adopted the migrated SRFs along that profile (Figure 7c) to examine the compatibility of the lithospheric structure with our models. Mohammadi et al. (2013) proposed that the thickness of the Arabian lithosphere beneath the Zagros is about 200 km, whereas the Iranian lithosphere is much thinner and the depth of LAB abruptly decreases to about 80-90 km beneath central Iran and Alborz (Figure 7c). A thickened lithosphere beneath the Zagros was also observed by Motaghi et al. (2017). Priestley et al. (2012) used multi-mode surface waves in order to map the lateral variations in the shear wave velocity of the upper mantle in the Middle East. They discovered a lithospheric root beneath the Zagros as thick as 225 km (Figure 7). The lithosphere thickness gradient was confirmed by Motavalli-Anbaran et al. (2011) and Jimenez-Munt et al. (2012). Tunini et al. (2015) applied a geophysical-petrological methodology and demonstrated that the depth of LAB abruptly decrease from about 220 km in the Zagros to about 120 km in central Iran and Alborz. Collectively, the results of these studies indicate that the lithospheric structure of the western Arabia-Eurasia collision zone is mostly in agreement with the slab break-off model (Figure 6a). Furthermore, there is strong evidence from P receiver function studies for crustal thickening caused by underplating of the Arabian continental crust under the overriding Iranian crust (Paul et al., 2010; Motaghi et al., 2017) (Figure 7). Magni et al. (2017) performed 3D numerical modeling to investigate the dynamics of continental collision and the fate of the subducted continental lithosphere. They showed that the continental subduction with a steep dip angle will be followed by a deep slab break-off. After that, the continental plate rises and is emplaced

under the overriding plate to form the thickened continental crust. Thus, the Tethyan slab break-off should have taken place prior to the underplating in the Arabia-Eurasia collision zone. The fact that underplating is the last step in the continental subduction process, suggests that the slab break-off scenario is more realistic. The variation of LAB depth estimated using the two-layer model with at least 1 sec delay time in each layer (the red model in Figure 5e) is also in good agreement with the lithospheric thickness reported by other studies (the undulated green dashed line in Figure 7c and d).

Tomographic images can also be used for interpretation of the observed shear wave splitting parameters. While there has been no high-resolution tomographic image of the region, the available global and regional scale studies suggest a high-velocity region beneath the Zagros in comparison with a low-velocity upper mantle beneath central Iran (Hafkenscheid et al., 2006; Vergés et al., 2011; Priestley et al., 2012). The P wave vertical tomographic transect of Vergés et al. (2011) shown in Figure 7d does not significantly differ from the tomographic transect presented by Hafkenscheid et al., (2006). The LAB depth suggested by Mohammadi et al. (2013) and Priestley et al. (2012) has been superimposed on the tomographic image. Apart from the high-velocity thick Arabian lithosphere which is clearly evident, there is another high-velocity region deeper than 450 km beneath the Zagros, SSZ and central Iran (Figure 7d). Roughly the same high-velocity region is evident in the Hafkenscheid et al. (2006) tomographic image. A two-stage Neo-Tethyan slab break-off is hypothesized by Hafkenscheid et al. (2006) and Agard et al. (2011). The Neo-Tethyan mid-ocean ridge reached the Eurasia margin in late Paleocene and the first slab break-off occurred almost simultaneously (Hafkenscheid et al., 2006; Agard et al., 2011). Given the global average sinking rate of 12±3 mm/yr (Van der Meer et al. 2010; Butterworth et al. 2014; Domeier et al. 2016) and the onset of the first slab break-off in late Paleocene, the first broken-off Neo-Tethyan slab (FBS) should be currently residing at more than 550 km depth. In that case, the deep high-velocity region beneath the Zagros, SSZ and central Iran could actually be representing the stagnant slab laid on the 660 km discontinuity (Figure 7d). The second slab break-off in eastern Zagros is believed to have occurred in late Miocene (Agard et al., 2011). Taking a break-off age of 10 Ma and the same global average slab sinking rate of the slab, the last broken-off slab (LBS) should be more than 100 km below the LAB. The width of the Neo-Tethys Ocean in the Middle Eocene was about 220 km (Agard et al., 2011) which suggests that the length of the LSB should approximately be the same. The thickness of oceanic lithosphere increases with age as it moves away from mid-ocean ridge. Furthermore, the first slab break-off and the consequent onset of the new subduction almost coincided with the time when the Neo-Tethyan mid-ocean ridge reached the Eurasian margins. Thus, the older end of the LSB and the younger end of the FBS should have been very thin and young. The younger end of the LSB could not have been very thick since it must had necked prior to break-off (Magni et al., 2017). Therefore, the LSB should be wide in the middle and tapered at both ends. Figure 7d shows the approximate forms and locations of the remnant Neo-Tethyan slabs.

3.3 Geodynamical Implication

3.3.1 2D Geodynamical Model of the Western Arabia-Eurasia Collision Zone

The results of the receiver function studies and tomographic images discussed in the previous section (Figure 7) suggest that the slab break-off model is more compatible with the geophysical observations. Our preferred 2D geodynamical model of the western part of the Arabia-Eurasia collision zone inferred from combination of shear wave splitting

measurements and the results of other geophysical studies is illustrated in Figure 8 and is summarized in the following.

In the western Zagros and SSZ, the oblique convergence between the Arabian plate and Eurasia has caused transpressional deformation which develops a deformation fabric that is characterized by vertical foliations and (sub)horizontal lineations. This particular fabric gives the mountain range-parallel shear wave splitting measurements. Several studies on Pn velocity structure (Al-Lazki et al., 2014; Lü et al., 2012: Lü et al., 2017) have investigated the variations of the azimuthal anisotropy of the Pn phase over the Iranian Plateau (see Figure 1b). Overall these studies show strong variations of Pn anisotropy at the depth of Moho over short distances, but in the region of our interest, Pn anisotropy is more or less parallel with the major structural trends (i.e. NW-SE). This is in agreement with the lithospheric origin of the mountain range-parallel anisotropy in the western Zagros (Figure 1b). The range-perpendicular asthenospheric flow beneath the thick deformed lithosphere in ZFTB and SSZ is not strong enough to dominate the lithospheric anisotropy. However, outside of the folded belt (on the foreland basin of the south of the Zagros and also to the north of SSZ in central Iran), thinning of the lithosphere along with the reduction of lithospheric deformation and its contribution to the apparent anisotropy can lead to the domination of the plate motion-parallel anisotropy caused by the sublithospheric flow field. The reduction in the lithospheric contribution to the anisotropy in the north of SSZ in central Iran is coherent with the decrease in the magnitude of Pn Anisotropy in that region (Figure 1b). In central Iran and to the south of Alborz the abrupt decrease in the lithospheric thickness may result in an EDC flow and edge-parallel fast-axis orientations. Apart from the EDC flow and the keel effect of the thickened Zagros lithosphere as sublithospheric causes, the lithospheric deformation localized along the major shear zones of central Iran can contribute to the observed NW-SE trend in central Iran (Lave et al., 1996; Kaviani et al., 2009). A shallow LAB and a dominant NE-SW trend parallel to the plate motion directions in eastern Turkey (Sandvol et al., 2003), northwest Iran (Arvin et al., 2014), central Alborz (Sadidkhouy et al., 2008) and to the northeast of Iran (Kaviani et al., 2009) show a continuation of the uniform NE-SW anisotropic structure from eastern Turkey into NW and northern Iran. This implies that the NE-SW fast-axis orientation originates from the asthenospheric flow.

3.3.2 Geodynamical Model of the Alborz: Variation of Lithospheric Deformation Pattern from East to West

The pattern of lithospheric deformation along the Alborz mountain belt could be influenced by the oroclinal bending process. In this case, the lithospheric contribution to the splitting parameters can be affected by the angle between Mountain belt trend and the convergence direction. The arcuate shape of the Alborz Mountains is related to the buttressing of the range between Central Iran and the South Caspian Basin (SCB) blocks (Allen et al., 2003; Shabanian et al., 2012; Mousavi et al., 2013). Therefore, the pattern of deformation in the Alborz is influenced by the geometry and relative motion of these blocks. The small number of GPS stations in the SCB, mostly at the southern margin, are insufficient to estimate true motion of central Iran relative to the SCB (Djamour et al., 2010; Mousavi et al., 2013). Nevertheless, the geodetic velocity field of the Alborz and SCB with respect to central Iran (Djamour et al., 2010) is consistent with the present-day kinematics of the Alborz Mountains deduced from both geological and seismological observations (Shabanian et al., 2012). We used the map of free-air gravity anomaly (http://icgem.gfz-potsdam.de) to determine the overall physiographic trend of the Alborz belt by picking the maximum anomaly values. A second-order polynomial was fitted to the smoothed trend (Figure 9a). The angle between the vector of southwestward motion of the SCB relative to central Iran

and the convergence interface (the Alborz trend) was calculated and it clearly shows the variation in convergence obliquity from an almost head-on collision in the western Alborz to an oblique convergence and even parallel motion in eastern Alborz (Figure 9b). Such variations lead to a change in the pattern of deformation (see also section 5.3). Accordingly, the frontal collision in the western Alborz would result in pure shear-dominated (PSD) lithospheric transpression that could produce deformational fabric with vertical lineations (Fossen et al., 1994; Tommasi, 1999). This fabric could result in apparent null splitting in the lithosphere, leaving the observed anisotropic signal to be dominated by the shear flow in the asthenosphere beneath. The negligible values of Pn anisotropy in the western Alborz (Lü et al., 2017) could be an evidence for the sublithospheric origin of the observed splittings (Figure 9a). In the central and eastern Alborz, the belt-parallel component of the relative motion increases and a simple shear-dominated (SSD) regime establishes. This kinematic change leads to a transition from transpressional to transtensional (TT) deformation regimes from the west to the east of the belt (Shabanian et al., 2012). The horizontal lineation and vertical foliation produced in SSD transpressional deformation (Fossen et al., 1994; Tommasi, 1999; Sullivan and Law, 2007; Baptiste and Tommasi, 2014) cause an aggregation of belt-parallel lithospheric and NNR-parallel asthenospheric splittings in central Alborz. Towards the eastern part of Alborz where the relative motion of SCB and central Iran are almost parallel with mountain trends, the deformation pattern changes to the SSD and PSD transtensional regimes. The horizontal lineation in these transtensional deformations (Fossen et al., 1994) in eastern Alborz may result in the deviation of anisotropic trend from the asthenospheric plate motion-parallel pattern observed in western Alborz. The idea of larger contribution from lithospheric anisotropy in central and eastern Alborz in comparison with western Alborz, is supported by the results of Pn anisotropy (Figure 9a). This transition from plate motion-parallel fast-axes in western Alborz to non-belt-perpendicular/belt-parallel pattern predicted for eastern Alborz can explain the contrasting results between Sadidkhouy et al. (2008) and Kaviani et al. (2009) in the Alborz.

3.3.3 Expansion to a 3D Geodynamical Model of the Arabia-Eurasia Collision Zone

Variable fast polarization orientations and the lithospheric thickness gradient across the western Arabia-Eurasia collision zone (Figure 7) are the main ingredients of the 2D geodynamical model presented in Figure 8. The large-scale study of Priestley et al. (2012) showed that the depth of LAB abruptly decreases to the west of our 2D model. Kind et al. (2015) utilized S receiver functions to estimate the lithospheric thickness of eastern Turkey. Their results agree with those of Priestley et al. (2012), implying that the lithosphere to the west of our 2D model is much thinner. The systematic difference between the fast-axis orientations of the western earthquakes and eastern earthquakes (Figure 3), discussed in section 2.1, can be considered as an indication of a dominant contribution of the asthenospheric flow in the anisotropic structure near the northern edge of the Arabia and to the south of the Bitlis suture. The results of the first Fresnel zone analysis at stations E01, M01, M04 and M06 in the Zagros (Figure 4, Figure S2) and comparison of the estimated depths of the anisotropic layer with the tomographic image and the migrated SRFs (Figure 7) are in agreement with the idea that the west-to-east anisotropic gradient should have its source in the deep structures. Therefore, the plate motion-parallel trend to the west of the 2D model can be associated to the asthenospheric flow beneath the Mosapotamian plain and the Zagros-parallel fast polarizations are the result of the transpressional deformation in the thickened lithosphere of the western Zagros (Figure 10).

To the southeast of the 2D model, the lithospheric thickness along the strike of the Zagros does not change significantly (Priestley et al., 2012; Mohammadi et al., 2013). Arabia

and Eurasia have an oblique convergent boundary. GPS velocity vectors in a Eurasia-fixed frame, however, show that the motion of Arabia relative to Eurasia changes along the collision boundary from a northward movement in western Zagros to a NNE trend in eastern Zagros (Walpersdorf et al., 2006). This variation along the suture belt results in an oblique convergence in western Zagros but approximately frontal in eastern Zagros (Jackson, 1992; Talebian and Jackson, 2002; Vernant and Chery, 2006). At crustal scale, the oblique convergence in western Zagros is partitioned to dextral and reverse movements on the Main Recent Fault (MRF) and the Mountain Frontal Fault (MFF), respectively (Jackson, 1992; Talebian and Jackson, 2002). This strain partitioning is not observed in eastern Zagros. At lithospheric scale, we believe that the oblique convergence is accommodated by ductile transpressional deformation in the lithospheric mantle. As discussed previously in the 2D model, the large suture-parallel component of convergence in western Zagros results in the domination of simple shear deformation and horizontal lineation fabrics (Figure 8 and 10). To the southeast and in central and eastern Zagros the suture-parallel component of the convergence decreases, hence the PSD transpression and axial shortening could lead to a more vertically-oriented lineations and a decrease in the strength of the mountain belt-parallel-splitting caused by lithospheric anisotropy (Fossen et al., 1994; Tommasi, 1999; Sullivan and Law, 2007; Baptiste and Tommasi, 2014) (Figure 10). Such a transition between different deformation regimes may give rise to deviation of the lithospheric splittings from the observable belt-parallel trend and even cause the domination of plate-motion-parallel fast-axis orientations originating from the asthenospheric flow filed in eastern Zagros. The variation of lithospheric anisotropy along the Zagros inferred from Pn anisotropy (Al-Lazki et al., 2014; Lü et al., 2012: Lü et al., 2017) provides an important clue to the predicted non-belt-parallel lithospheric anisotropy in the eastern Zagros.

4 Conclusions

The individual splitting measurements obtained from the dense temporary profile of 63 broadband seismic stations in the western part of the Arabia-Eurasia collision zone are critically analyzed. The results show that the fast-axis orientations dramatically rotate along the profile. A 2D geodynamical model justifying the observed anisotropic variations crossing the western Zagros, central Iran and western Alborz has been proposed (Figure 8):

- The belt-parallel fast-axis trend observed in the western Zagros originates from a lithospheric transpressional deformation;
- The belt-perpendicular (plate motion-parallel) fast-axis orientations in central Iran and western Alborz are a result of a sublithospheric mantle flow;
- The keel effect of the thickened Zagros lithosphere together with the edge-driven convection flow produced by the lithospheric thickness gradient are the causative asthenospheric mechanisms behind the NW-SE anisotropic pattern in central Iran. Apart from the sublithospheric causes, deformation in the central Iran major shear zones also contributes to the observed anisotropy.

The GPS velocity vectors along the Alborz and Zagros convergence boundaries were examined to measure the convergence directions and relative motion of the plates. The variation of the convergence obliquity along the Alborz and Zagros implies that a change in the pattern of lithospheric deformation is expected, which in turn influences the seismic anisotropy:

- The variation in the pattern of lithospheric deformation along the Alborz can cause the fast-axis orientations to shift from the asthenospheric plate motion-

parallel trend in western Alborz to a lithospheric and/or asthenospheric non-belt-perpendicular/belt-parallel pattern in eastern Alborz;

- A shift from lithospheric belt-parallel pattern in the western Zagros to an asthenospheric plate motion-parallel trend in the eastern Zagros is probable.

The observed plate motion-parallel fast-axis orientations to the west of the 2D model have their origin in the sublithospheric flow beneath the thin lithosphere in northern Iraq.

Acknowledgments

Amir Sadeghi-Bagherabadi acknowledges support from the TRIL programme (ICTP-INGV agreement) and from the ICTP-Regione Friuli-Venezia Giulia programme. All the data used are listed in the supplementary material Table S1. This work is done in the framework of the collaboration between the Chinese Academy of Sciences, Geological Survey of Iran and Institute for Advanced Studies in Basic Sciences. The authors appreciate helpful discussions with Francesco Pio Lucente, Paola Baccheschi, Carlo Doglioni, Esmaeil Shabanian and Iman Monsef. Two anonymous reviews are thanked for thoughtful comments which significantly improved the paper.

References

Abramson, E. H., J. M. Brown, L. J. Slutsky, and J. Zaug (1997), The elastic constants of San Carlos olivine to 17 GPa, J. Geophys. Res., 102(B6), 12253-12263.

Agard P, J. Omrani, L. Jolivet, H. Whitechurch, B. Vrielynck, W. Spakman, P. Monie, B. Meyer, and R. Wortel (2011), Zagros orogeny: a subduction-dominated process, Geol Mag 148:692–725

Alavi, M., (1994), Tectonics of the Zagros orogenic belt of Iran: new data and interpretations. Tectonophysics, 229, 211–38.

Al-Lazki, A., K. S. Al-Damegh, S. Y. El-Hadidy, A. Ghods and M. Tatar (2014), Pn-velocity structure beneath Arabia−Eurasia Zagros collision and Makran subduction zones. Geological Society, London, Special Publications, 392; 45-60. doi: 10.1144/SP392.3

Allen M.B., Vincent S. J., Alsop. G. I., and Ismail-zadeh. A., Flecker. R., (2003), Late Cenozoic deformation in the South Caspian region: effects of a rigid basement block within a collision zone: Tectonophysics 366, 223-239p.

Allen MB, and H.A. Armstrong (2008), Arabia–Eurasia collision and the forcing of mid-Cenozoic global cooling, Paleogeogr Paleoclimatol Paleoecol 265:52–58

Alsina, D., and R. Snieder (1995), Small-scale sublithospheric continental mantle deformation; constraints from SKS splitting observations, Geophys. J. Int., 123, 431– 448, 1995.

Arvin, S., F. Sobouti, A. Ghods, G. Mortezanejad, and K. Priestley (2014), Study of seismic anisotropy in NW Iran, in: Proceedings of the 16th Iranian Geophysical Conference, May 2015, Tehran, Iran. p 130-134.

Baccheschi, P., L. Margheriti, and M. Steckler (2007), Seismic anisotropy reveals focused mantle flow around the Calabrian slab (southernItaly), Geophys. Res. Lett. 34, doi:10.1029/2006gl028899

Baccheschi, P., M. Pastori, L. Margheriti, and D. Piccinini (2016), Shear wave splitting of the 2009 L'Aquila seismic sequence: fluid saturated microcracks and crustal fractures in the Abruzzi region (Central Apennines, Italy), Geophys. J. Int., 204, 1531–1549.

Ballato, P., C.E. Uba, A. Landgraf, M.R. Strecker, M. Sudo, D.F. Stockli, A. Friedrich, and S.Tabatabaei (2011), Arabia-Eurasia continental collision: Insights from late Tertiary

foreland-basin evolution in the Alborz Mountains, northern Iran, GSA Bulletin, 123, 106–13, doi: 10.1130/B30091.1.

Baptiste, V. and A. Tommasi (2014) Petrophysical constraints on the seismic properties of the Kaapvaal craton mantle root, Solid Earth, 5, 45-63, doi:10.5194/se-5-45-2014, 2014.

Barruol, G., M. Bonnin, H. Pedersen, G. Bokelmann, and C. Tiberi (2011), Belt-parallel mantle flow beneath a halted continental collision: the western Alps, Earth Planet. Sci. Lett., 302, 429–438, doi:10.1016/j.epsl.2010.12.040.

Bokelmann, G., E. Qorbani, and I. Bianchi (2013), Seismic anisotropy and large-scale deformation of the Eastern Alps, Earth Planet. Sci. Lett., 383, 1–6, doi:10.1016/j.epsl.2013.09.019.

Butterworth, N.P., A.S. Talsma, R.D. Müller, M. Seton, H.-P. Bunge, B.S.A. Schuberth, G.E. Shephard, and C. Heine (2014), Geological, tomographic, kinematic and geodynamic constraints on the dynamics of sinking slabs, JOURNAL OF GEODYNAMICS, 73, 1-13, doi:10.1016/j.jog.2013.10.006.

Civello, S., Margheriti, L., 2004. Toroidal mantle flow around the Calabrian slab (Italy) from SKS splitting. Geophys. Res. Lett. 31, L10601, doi:10.1029/ 2004GL019607.

Cızkova, H., A. P. van den Berg, W. Spakman, and C. Matyska (2012), The viscosity of Earth's lower mantle inferred from sinking speed of subducted lithosphere, Phys. Earth Planet. Inter., 200–201, 56–62, doi:10.1016/j.pepi.2012.02.010. Cl

Crosson, R.S., and J.W., Lin (1971), Voigt and Reuss prediction of anisotropic elasticity of olivine: J. Geophys. Res., 76(4), 570-578.

Davis, J. C., (1986), Statistics and Data Analysis in Geology, John Wiley & Sons Ltd., West Sussex.

Dewey, J.F., W.C. Pitman, W.B.F. Ryan, and J. Bonnin (1973), Plate tectonics and the evolution of the alpine system, Geol. Soc. Am. Bull. 84:3137–3180

Djamour, Y., Vernant, P., Bayer, R., Nankali, H. R., Ritz, J. F., Hinderer, J., … Khorrami, F. (2010). GPS and gravity constraints on continental deformation in the Alborz mountain range, Iran. Geophysical Journal International, 183(3), 1287–1301, doi:10.1111/j.1365-246X.2010.04811.x

Domeier, M., V. Doubrovine, T.H. Torsvik, W. Spakman, and A. Bull (2016), Global correlation of lower mantle structure and past subduction. Geophysical Research Letters 43, 4945- 4953.

Faccenda, M., F.A. Capitanio (2012), Development of mantle seismic anisotropy during subduction-induced 3-D flow, Geophys. Res. Lett.39, L11305.

Fontaine, F.R., G. Barruol, A. Tommasi, and G.H.R. Bokelmann (2007), Upper-mantle flow beneath French Polynesia from shear wave splitting. Geophys, J. Int.170, 1262–1288, doi:10.1111/j.1365-246X.2007.03475.x.

Fossen, H., B. Tikoff, and C.T. Teyssier (1994), Strain modeling of transpressional and transtensional deformation. Norsk Geologisk Tidsskrift, Vol. 74, pp. 134-145. Oslo, JSSN 0029-196X.

Fry, B., F. Deschamps, E. Kissling, L. Stehly, and D. Giardini (2010), Layered azimuthal anisotropy of Rayleigh wave phase velocities in the European Alpine lithosphere inferred from ambient noise, Earth Planet. Sci. Lett. 297 (1), 95–102.

Gao, S.S., and K. Hh. Liu, (2012) AnisDep: a FORTRAN program for the estimation of the depth of anisotropy using spatial coherency of shear-wave splitting parameters. Comput. Geosci., doi:10.1016/j.cageo.2012.01.020.

Hafkenscheid, E., M. J. R. Wortel, and W. Spakman (2006), Subduction history of the Tethyan region derived from seismic tomography and tectonic reconstructions, J. Geophys. Res., 111, B08401, doi:10.1029/2005JB003791.

Hempton, M.R., (1987), Constraints on Arabian Plate motion and extensional history of the Red Sea, Tectonics 6:687–705

Hill, R., (1952), The elastic behaviour of a crystalline aggregate, Proceedings of the Physics Society A 65, 349–354.

Huang, T.-Y., Y. Gung, B.-Y. Kuo, L.-Y. Chiao, and Y.-N. Chen (2015), Layered deformation in the Taiwan orogeny, Science 349, 720–7233, doi:10.1126/science.aab1879.

Jackson, J. (1992), Partitioning of strike-slip and covergent motion between Eurasia and Arabia in eastern Turkey and the Caucasus. J. Geophys. Res., 97, 12 471–12 479.

Jim´enez-Munt, I., M. Fern`andez, E. Saura, J. Verg´es, and D. Garc´ıa-Castellanos (2012), 3D lithospheric structure and regional/residual Bouguer anomalies from Arabia-Eurasia collision (Iran), Geophys. J. Int., 190, 1311– 1324.

Kaislaniemi, L., and J. van Hunen (2014), Dynamics of lithospheric thinning and mantle melting by edgedriven convection: Application to Moroccan Atlas Mountains, Geochem. Geophys. Geosyst., 15, 3175–3189, doi:10.1002/2014GC005414.

Kaviani, A., D. Hatzfeld, A. Paul, M. Tatar, and K. Priestley (2009), Shear wave splitting, lithospheric anisotropy, and mantle deformation beneath the Arabia-Eurasia collision zone in Iran, Earth Planet. Sci. Lett., 286, 371–378, doi:10.1016/j.epsl.2009.07.003.

Khadivi, S., F. Mouthereau, J. Barbarand, T. Adatte, and O. Lacombe (2012), Constraints on palaeodrainage evolution induced by uplift and exhumation on the southern flank of the Zagros-Iranian Plateau, J. Geol. Soc. 169:83–97

Kind, R., T. Eken, F. Tilmann, F. Sodoudi, T. Taymaz, F. Bulut, X. Yuan, B. Can, and F. Schneider (2015), Thickness of the lithosphere beneath Turkey and surroundings from S-receiver functions. Solid Earth, 6, 971–984, doi:10.5194/se-6-971-2015.

King, S. D. and D. L. Anderson (1998), Edge-driven convection, Earth Planet. Sci. Lett., 160(3-4), 289–296.

Lave, J., J.P. Avouac, R. Lacassin, P. Tapponnier, and J.P. Montagner (1996), Seismic anisotropy beneath Tibet; evidence for eastward extrusion of the Tibetan lithosphere? Earth Planet. Sci. Lett., 140, 83-96.

Liu, K. H. and S. S. Gao (2011), Estimation of the Depth of Anisotropy Using Spatial Coherency of Shear-Wave Splitting Parameters. Bull. Seismol. Soc. Am., 101 (5): 2153–2161, doi:10.1785/0120100258

Long, M. D., and T. W. Becker (2010), Mantle dynamics and seismic anisotropy. Earth and Planetary Science Letters, 297(3–4), 341–354, doi:10.1016/j.epsl.2010.06.036

Lü, Y., B. Liu, S. Pei, Y. Sun, M. N. Toksöz, and X. Zeng (2012), Pn Tomographic Velocity and Anisotropy beneath the Iran Region, Bull. Seismol. Soc. Am., 102, 426–435, doi: 10.1785/0120100141

Lü, Y., S. Ni, L. Chen, and Q.-F. Chen (2017), Pn tomography with Moho depth correction from eastern Europe to western China, J. Geophys. Res. Solid Earth, 122, 1284–1301, doi:10.1002/2016JB013052.

Magni, V., M.B. Allen, J. van Hunen, and P. Bouilhol (2017), Continental underplating after slab break-off. Earth Planet. Sci. Lett. 474, 59–67, doi:10.1016/ j.epsl.2017.06.017.

Mainprice, D., (1990), A fortran program to calculate seismic anisotropy from the lattice preferred orientation of minerals, Computers and Geosciences 16, 385–393.

Mainprice, D., A. Tommasi, H. Couvy, P. Cordier (2005), Pressure sensitivity of olivine slip systems and seismic anisotropy of earth's upper mantle, Nature, 433, 731–733, doi:10.1038/nature 03266.

Mardia, K. V., and P. E. Jupp (2000), Directional Statistics. John Wiley & Sons Ltd., West Sussex.

Margheriti, L., F. P. Lucente, and S. Pondrelli (2003), SKS Splitting measurements in the Appenninic-Tyrrhenian domains (Italy) and their relation with Litospheric subduction and mantle convection, J. Geophys. Res., 108(B4), 2218, doi:10.1029/2002JB001793.

Margheriti, L., C. Nostro, M. Cocco, and A. Amato, (1996), Seismic anisotropy beneath the Northern Apennines (Italy) and its tectonic implications, Geophys. Res. Lett. 23 (20), 2721–2724, doi.org/10.1029/96GL02519.

Meissner, R., W.D. Mooney, and I. Artemieva (2002), Seismic anisotropy and mantle creep in young orogens, Geophys. J. Int., 149, 1–14.

Mohammadi, E., F. Sodoudi, R. Kind, and M. Rezapour (2013), Presence of a layered lithosphere beneath the Zagros collision zone, Tectonophysics, 608, 366–375.

Moradi, P., F. Sobouti, A. Ghods, K. Motaghi, K. Priestley (2015), Seismic anisotropy and shear wave splitting in western Alborz and adjacent regions, in: Proceddings of 7th International Conference on Seismology and Earthquake Engineering, 18-21 May 2015, Tehran, Iran.

Motaghi, K., E. Shabanian, and F. Kalvandi (2017), Underplating Along the Northern Portion of the Zagros Suture Zone, Iran, Geophys. J. Int., 210, 375–389, doi:10.1093/gji/ggx168

Motavalli-Anbaran, S.-H., H. Zeyen, M.-F. Brunet, and V.E. Ardestani (2011), Crustal and lithospheric structure of the Alborz Mountains, Iran, and surrounding areas from integrated geophysical modeling, Tectonics, 30, TC5012, doi:10.1029/2011TC002934.

Mousavi, Z., Walpersdorf, A., Walker, R. T., Tavakoli, F., Pathier, E., Nankali, H., Djamour, Y. (2013). Global Positioning System constraints on the active tectonics of NE Iran and the South Caspian region. Earth and Planetary Science Letters, 377-378, 287–298.\, doi:10.1016/j.epsl.2013.07.007

Mouthereau, F., J. Tensi, N. Bellahsen, O. Lacombe, T. De Boisgrollier, and S. Kargar (2007), Tertiary sequence of deformation in a thin-skinned/thick-skinned collision belt: The Zagros Folded Belt (Fars, Iran), Tectonics, 26, TC5006, doi:10.1029/2007TC002098.

Mouthereau, F., O. Lacombe, and J. Vergés (2012), Building the Zagros collisional orogen: Timing, strain distribution and the dynamics of Arabia/Eurasia plate convergence, Tectonophysics, 532–535, 27–60, doi:10.1016/j.tecto.2012.01.022.

Nicolas, A., (1993) Why fast polarization directions of SKS seismic waves are parallel to mountain belts, Phys. Earth Planet. Inter., 78, 337–342.

Omrani, J., P. Agard, H. Whitechurch, M. Benoit, G. Prouteau, and L. Jolivet (2008), Arc-magmatism and subduction history beneath the Zagros Mountains, Iran: Anewreport of adakites and geodynamic consequences. Lithos 106, 380–98.

Ozacar, A.A., and G. Zandt (2004), Crustal seismic anisotropy in central Tibet: implications for deformational style and flow in the crust, Geophys. Res. Lett. 31, L23601.

Paul, A., A. Kaviani, D. Hatzfeld, M. Tatar, and C. Pequegnat (2010), Seismic imaging of the lithospheric structure of the Zagros mountain belt (Iran), in Tectonic and Stratigraphic Evolution of Zagros and Makran During the Meso-Cenozoic, vol. 330, pp. 5–18, eds Leturmy, P. & Robin, C., Geological Society, Special Publications.

Priestley, K., D. McKenzie, J. Barron, M. Tatar, and E. Debayle (2012), The Zagros core: deformation of the continental lithospheric mantle, Geochem. Geophys. Geosyst. 13, Q11014., doi:10.1029/2012GC004435.

Qorbani, E., I. Bianchi, and G. Bokelmann (2015), Slab detachment under the Eastern Alps seen by seismic anisotropy, Earth Planet. Sci. Lett., 409, 96–108, doi:10.1016/j.epsl.2009.07.003.

Sadeghi-Bagherabadi, A., F. Sobouti, A. Ghods, K. Motaghi, M. Talebian, L. Chen, M. Jiang, Y. Ai, and Y. He (2018), Upper Mantle Anisotropy and Deformation beneath the Major Thrust-and-Fold Belts of Zagros and Alborz and the Iranian Plateau, Geophys. J. Int., doi:10.1093/gji/ggy233

Sadidkhouy, A., G. Javan-Doloei, and H. R. Siahkoohi, (2008), Seismic anisotropy in the crust and upper mantle of the Central Alborz Region, Iran, Tectonophysics, 456, 194–205, doi:10.1016/j.tecto.2008.05.001.

Salimbeni, S., S. Pondrelli, L. Margheriti, J. Park, and V. Levin (2008), SKS splitting measurements beneath Northern Apennines region: A case of oblique trench-retreat, Tectonophysics, 462(1–4), 68–82, doi:10.1016/j.tecto.2007.11.075.

Salimbeni, S., S. Pondrelli, and L. Margheriti (2013), Hints on the deformation penetration induced by subductions and collision processes: Seismic anisotropy beneath the Adria region (Central Mediterranean), J. Geophys. Res. Solid Earth, 118, 5814–5826, doi:10.1002/2013JB010253.

Salimbeni, S., M. G. Malusà, L. Zhao, S. Guillot, S. Pondrelli, L. Margheriti, A. Paul, S. Solarino, C. Auberte, T. Dumont, S. Schwartz, Q. Wang, X. Xu, T. Zheng and R. Zhu (2018), Active and fossil mantle flows in the western Alpine region unravelled by seismic anisotropy analysis and high resolution P wave tomography. Tectonophysics, 731–732, 35-47, doi:10.1016/j.tecto.2018.03.002

Sandvol, E., N. Turkelli, E. Zor, R. Gok, T. Bekler, C. Gurbuz, D. Seber, and M. Barazangi (2003) Shear wave splitting in a young continent-continent collision: An example from Eastern Turkey, Geophys. Res. Lett., 30, 8041, doi:10.1029/2003GL017390, 24.

Saura, E., D. Garcia-Castellanos, E. Casciello, V. Parravano, A. Urruela, and J. Verges (2015), Modeling the flexural evolution of the Amiran and Mesopotamian foreland basins of NW Zagros (Iran–Iraq), Tectonics 34:377–395

Savage, M.K., (1999), Seismic anisotropy and mantle deformation: what have we learned from shear wave splitting? Rev. Geophys., 37 (1), 65–106, doi:10.1029/98RG02075.

Schmid, C., S. van der Lee, and D. Giardini (2004), Delay times and shear wave splitting in the Mediterranean region, Geophysical Journal International, 159, 275–290, doi:10.1111/j.1365-246X.2004.02381.

Shabanian, E., V. Acocella, A. Gioncada, H. Ghasemi, and O. Bellier (2012), Structural control on volcanism in intraplate post collisional settings: Late Cenozoic to Quaternary examples of Iran and Eastern Turkey, Tectonics, 31, TC3013, doi:10.1029/2011TC003042.

Silver, P. G., (1996) Seismic anisotropy beneath the continents: probing the depths of geology, Annu. Rev. Earth Planet. Sci. 24, 385–432.

Silver, P., and W. Chan, (1991), Shear wave splitting and subcontinental mantle deformation,J. Geophys, Res., 96, 16429–16454.

Song, T., and H. Kawakatsu, (2012), Subduction of oceanic asthenosphere: evidence from sub-slab seismic anisotropy, Geophys. Res. Lett.39, L17301.

Song, T.-R.A., and H. Kawakatsu, (2013), Subduction of oceanic asthenosphere: acritical appraisal in central Alaska, Earth Planet. Sci. Lett.367, 82–94.

Stoneley, R., (1981), The geology of the Kuh-e Dalneshin area of southern Iran, and its bearing on the evolution of southern Tethys, J. Geol. Soc. 138:509–526

Sullivan, W.A., and R.D. Law (2007), Deformation path partitioning within the transpressional White Mountain shear zone, California and Nevada, J. Struct. Geol., 29, 583-599, doi:10.1016/j.jsg.2006.11.001.

Talebian, M. and J. Jackson (2002), Offset on the main recent fault of NW Iran and implications for the late Cenozoic tectonics of the Arabia-Eurasia collision zone. Geophys. J. Int. 150, 422-439.

Talebian, M., and J. Jackson (2004), A reappraisal of earthquake focal mechanisms and active shortening in the Zagros mountains of Iran, Geophys. J. Int. 156:506–526

Tommasi, A., B. Tikoff, and A. Vauchez (1999), Upper mantle tectonics: three-dimensional deformation, olivine crystallographic fabrics and seismic properties, Earth Planet. Sci. Lett., 168, 173-186, doi:10.1016/S0012-821X(99)00046-1.

Tunini L., I. Jiménez-Munt, M. Fernandez, J. Vergés, and A. Villaseñor (2015), Lithospheric mantle heterogeneities beneath the Zagros Mountains and the Iranian Plateau: a petrological-geophysical study, Geophys. J. Int. 200:596–614, doi:10.1093/gji/ggu418.

Van der Meer, D.G., W. Spakman, D.J.J. van Hinsbergen, M.L. Amaru, and T.H. Torsvik, (2010), Towards absolute plate motions constrained by lower-mantle slab remnants. Nature Geoscience 3, 36–40.

Vergés, J., E. Saura, E. Casciello, M. Fernandez, A. Villasenor, I. Jimenez-Munt, and D. Garcia-Castellanos (2011), Crustal-scale cross-sections across the NW Zagros belt: Implications for the Arabian margin reconstruction, Geol. Mag., 148(5/6), 739–761.

Vernant, P., Chery, J., 2006. Mechanical modelling of oblique convergence in the Zagros, Iran. Geophysical Journal International 165 (3), 991–1002.

Walker, K.T., G.H.R. Bokelmann, S.L. Klemperer, and G. Bock (2005), Shear-wave splitting around the Eifel hotspot: evidence for a mantle upwelling, Geophys. J. Int.163, 962–980, doi:10.1111/j.1365-246X.2005.02636.x.

Walker, A. M., and J. Wookey (2012), MSAT — A new toolkit for the analysis of elastic and seismic anisotropy, Computers & Geosciences 49, 81–90, doi:10.1016/j.cageo.2012.05.031

Walpersdorf, A., D. Hatzfeld, H. Nankali, F. Tavakoli, F. Nilforoushan, M. Tatar, P. Vernant, J. Chéry, and F. Masson (2006), Difference in the GPS deformation pattern of North and Central Zagros (Iran). Geophys. J. Int., 167 (3), 1077, doi:10.1111/j.1365-246X.2006.03147.x.

Walpole, J., J. Wookey, J.M. Kendall, and T.G. Masters, (2017), Seismic anisotropy and mantle flow below subducting slabs, Earth Planet. Sci. Lett., 465, 155–167, doi:10.1016/j.epsl.2017.02.023

Wölbern, I., U. Löbl, and G. Rümpker (2014), Crustal origin of trench-parallel shear-wave fast polarizations in the Central Andes, Earth Planet. Sci. Lett., 392, 230–238, doi:10.1016/j.epsl.2014.02.032

Zandt, G., and E. Humphreys, (2008) Toroidal mantle flow through the western U.S. slab window, Geology36 (4), 295–298.

Zhang, Z., W. Xiao, M.R., Majidifard, R. Zhu, B. Wan, S. Ao, L. Chen, M. Rezaeian, and R. Esmaeili (2016), Detrital zircon provenance analysis in the Zagros Orogen, SW Iran: implications for the amalgamation history of the Neo-Tethys, Int. J. Earth Sci., doi:10.1007/s00531-016-1314-3

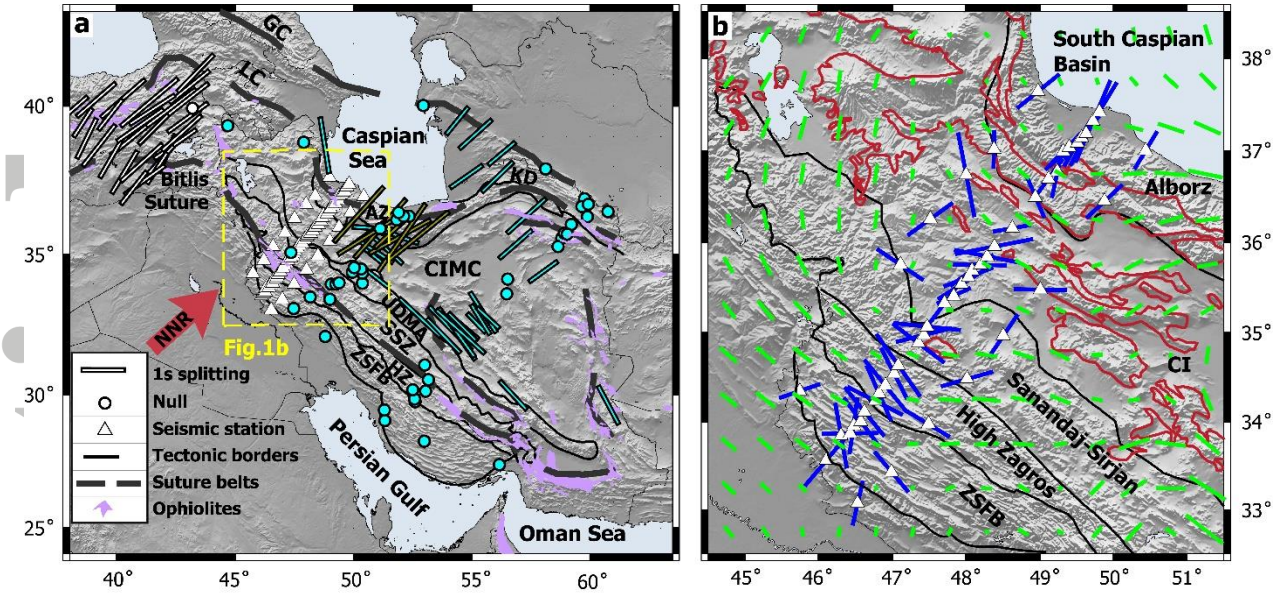

Figure 1. (**a**) Map of the Arabia-Eurasia collision zone and the shear wave splitting results of Sandvol et al. (2003) in eastern Turkey, Kaviani et al. (2009) and Sadidkhouy et al. (2008) in Iran (white, cyan and yellow symbols, respectively). Ophiolites and the probable suture belts are plotted. The box area is the frame of Figure 1b and Figure 2. (**b**) Triangles show the temporary seismic network used in this study. Blue bars are the average splitting results at each station, measured by Sadeghi-Bagherabadi et al. (2018). Green bars illustrate the Pn anisotropy measurements (Lü et al., 2017) and red lines mark the outcrop regions of the major volcanic and intrusive rocks. Abbreviations are defined as follows: ZSFB, Zagros Simply Folded Belt; HZ, High Zagros; SSZ, Sanandaj-Sirjan Zone; UDMA, Urmieh-Dhokhtar Magmatic Arc; CIMC, Central Iran Micro Continent; AZ, Alborz; KD, Kopet Dagh.

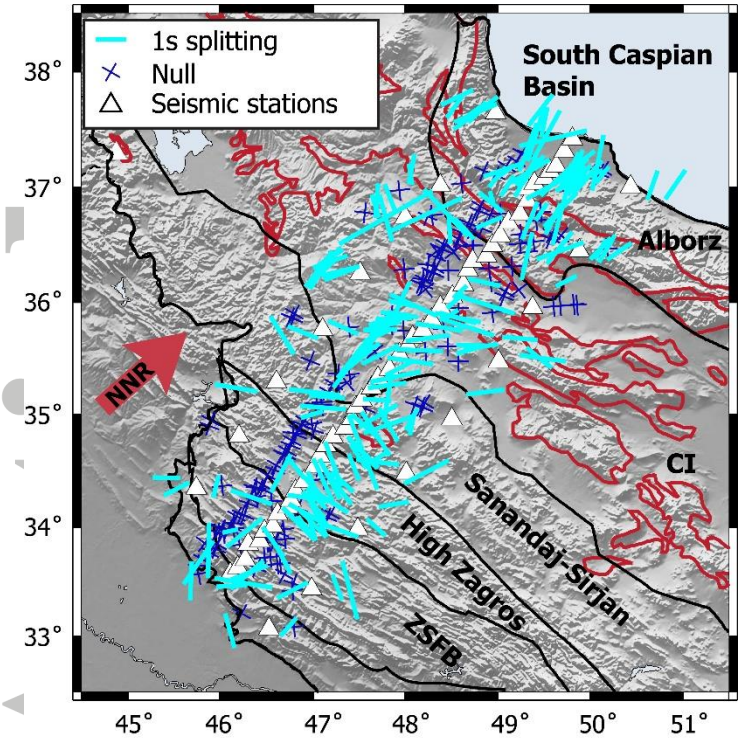

Figure 2. Map showing the individual splitting measurements projected down to the 150 km depth piercing points (cyan bars). The symbols (blue crosses) representing the null measurements are rotated through the back-azimuth of the earthquakes. Red lines mark the outcrop regions of the major volcanic and intrusive rocks which coincide with Urmieh-Dhokhtar Magmatic Arc (UDMA) to the east. Abbreviations are defined as follows: ZSFB, Zagros Simply Folded Belt; NNR, No-Net-Rotation; CI, Central Iran.

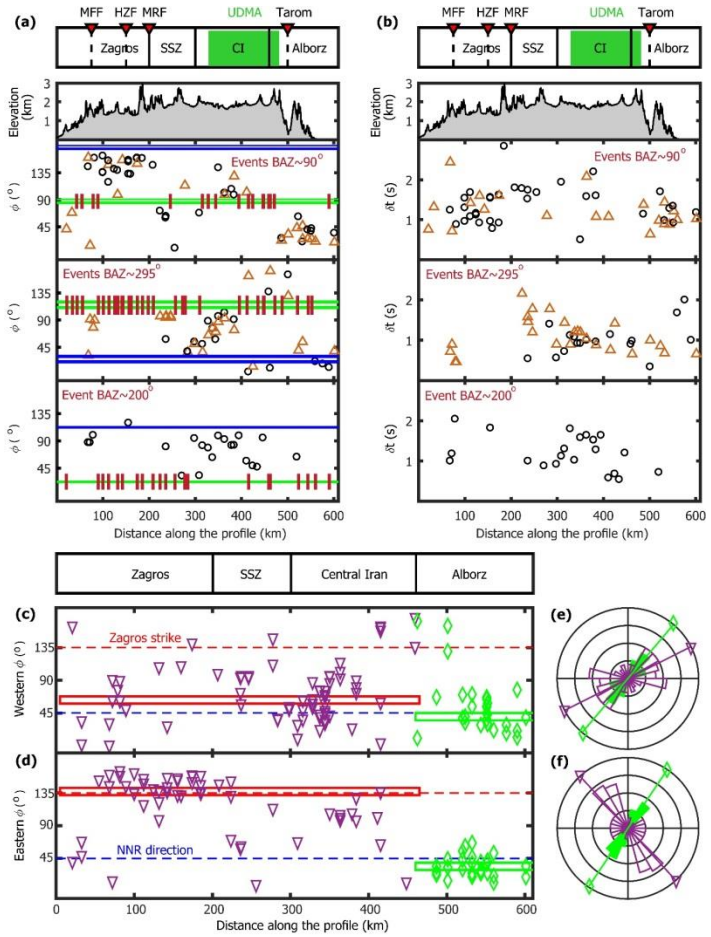

Figure 3. (**a**) The fast-axis orientations of seven events with back-azimuths between 84° and 90°, two events with back-azimuths of 291° and 300° as well as one earthquake with back-azimuth of 200°, projected along the middle profile of the seismic network. Green and blue lines are aligned with the backazimuth directions and the perpendicular directions, respectively. Vertical small red lines represent null measurements. (**b**) The delay times of the same events as (**a**). In each panel the best-recorded earthquakes are shown by brown triangles and the rest of the measurements by circles. The two top panels in each column illustrate the approximate locations of the main geological and structural boundaries and the topographic section along the profile. The main geological features are: Mountain Frontal Fault (MFF); High Zagros Fault (HZ); Main Recent Fault (MRF); Sanandaj-Sirjan Zone (SSZ); Central Iran (CI); Urmieh-Dhokhtar Magmatic Arc (UDMA) and the Tarom Valley. The fast-axis orientation of all earthquakes with back-azimuths greater than 180° and those with back-azimuths smaller than 180° are plotted in (**c**) and (**d**), respectively. The measurements obtained from Alborz stations are marked by green diamonds and those obtained from stations outside Alborz are shown by purple inverted triangles. Their circular average orientations are shown by colored bars. The no-net-rotation (NNR) direction and Zagros-strike in both (**c**) and (**d**) panels are shown by blue and red dashed lines, respectively. The rose diagrams corresponding to the fast-axis orientations plotted in (**c**) and (**d**) are illustrated in (**e**) and (**f**), respectively. The circular average values of the Alborz (green diamond) measurements and those of outside Alborz (purple triangle) are also plotted.

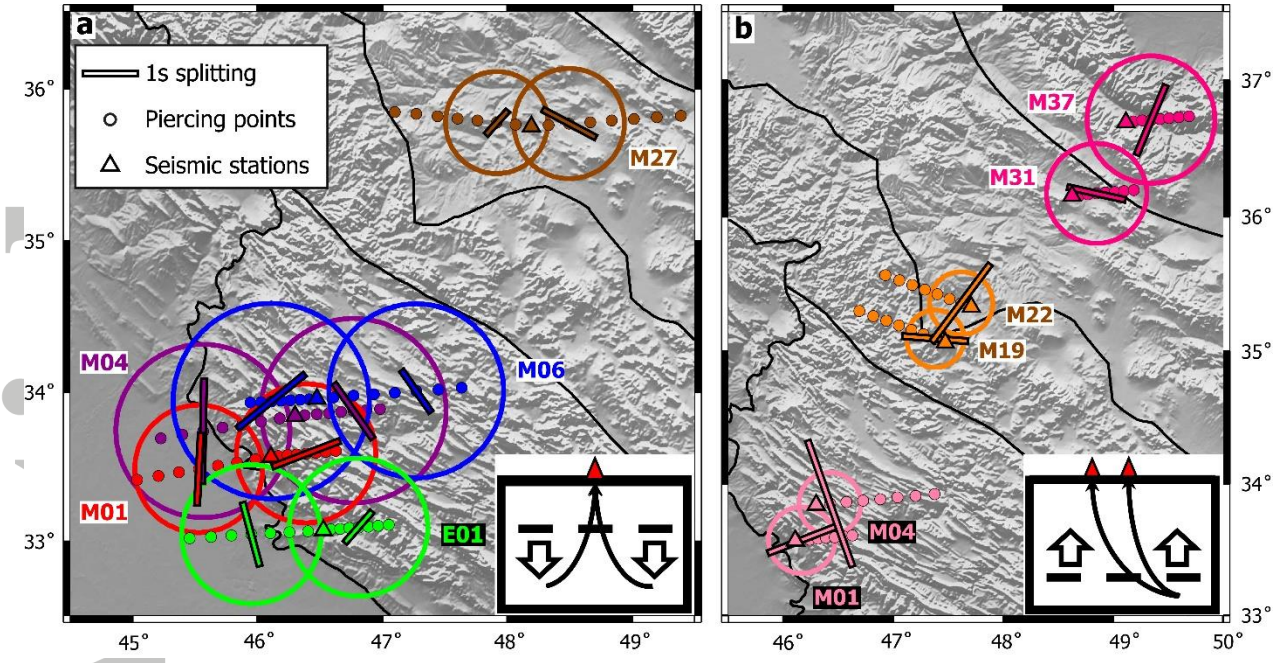

Figure 4. The first Fresnel zones (circles) of a set of selected earthquakes studied. Colored dots show the surface projection of the piercing points along ray paths at depths of 50 to 350 km. (**a**) Piercing points of pairs of earthquake ray paths with opposite back-azimuths at stations E01, M01, M04, M06 and M27 along with the Fresnel zones with maximum 10% overlap. (**b**) Same information as in (**a**) but for pairs of nearby stations receiving the same earthquake. In both maps the splitting measurements are plotted at the piercing depth that gives the 10% Fresnel zone overlap. The cartoon inserts illustrate the simplified geometry of the incoming rays and the depth at which the 10% overlap is achieved.

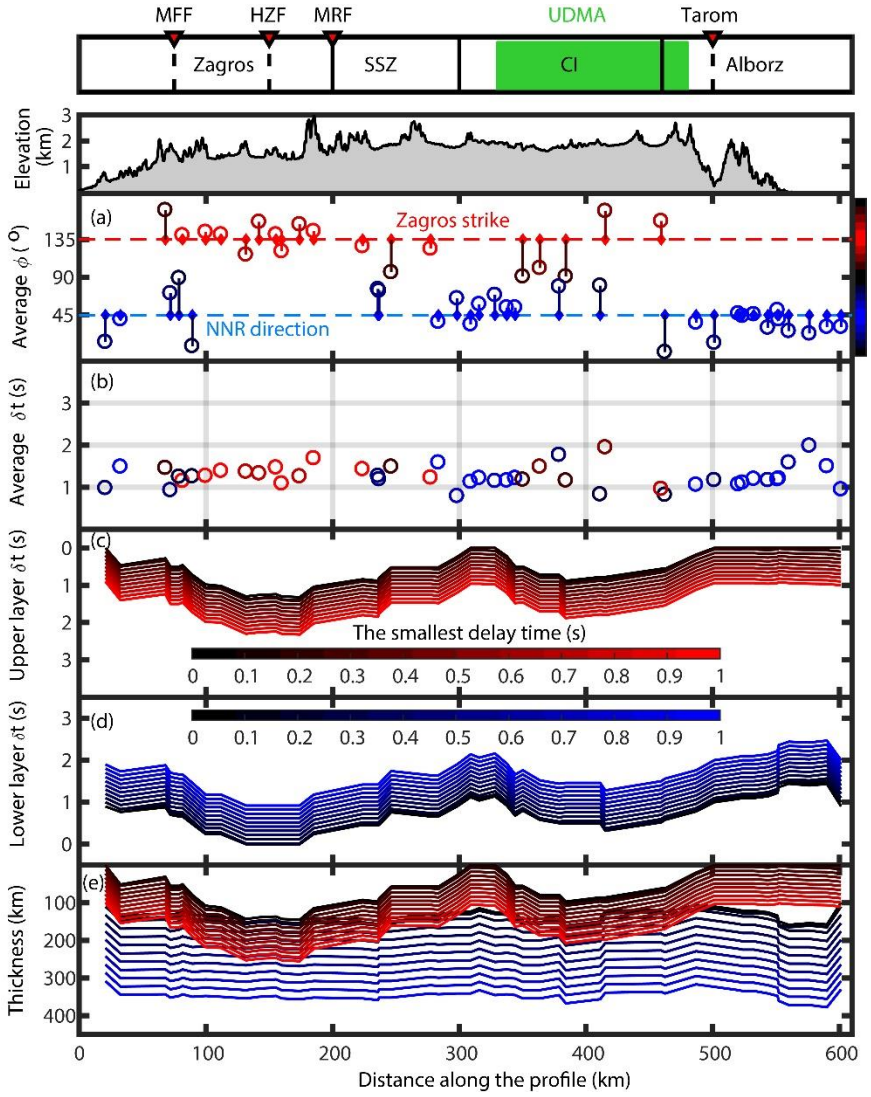

Figure 5. The results of two-layer modeling on the measurements. The two top rows and abbreviations are the same as Figure 3. (**a**) The bidirectional circular average fast-axis orientations (Equation 1) observed at stations are projected along the middle seismic profile. The Zagros strike (azimuth 135^{o}) and the no-net-rotation (NNR) absolute plate motion direction (azimuth 45^{o}) are marked by red and blue dashed lines, respectively. The color of each fast-axis symbol is according to the color bar on the right side; blue for matching with the NNR direction and red for matching with the Zagros strike. For the purpose of modeling each fast-axis observation was approximated with either the 45^{o} or 135^{o} direction. Vertical arrows on the symbols show this shift. (**b**) Average delay times at stations plotted with same color bar in panel (**a**). (**c** and **d**) Smoothed trends of delay times in the upper and lower layers of the best-fitting two-layer models, respectively. Note the opposite directions in the time axes between the two panels. Black trends in both panels represent the models in which the delay time in the layer with weaker anisotropy is about zero (isotropic). Towards the blue or red trends the delay time increases to 1 sec. (**e**) The thickness of the two layers converted from the trend of the modeled delay times.

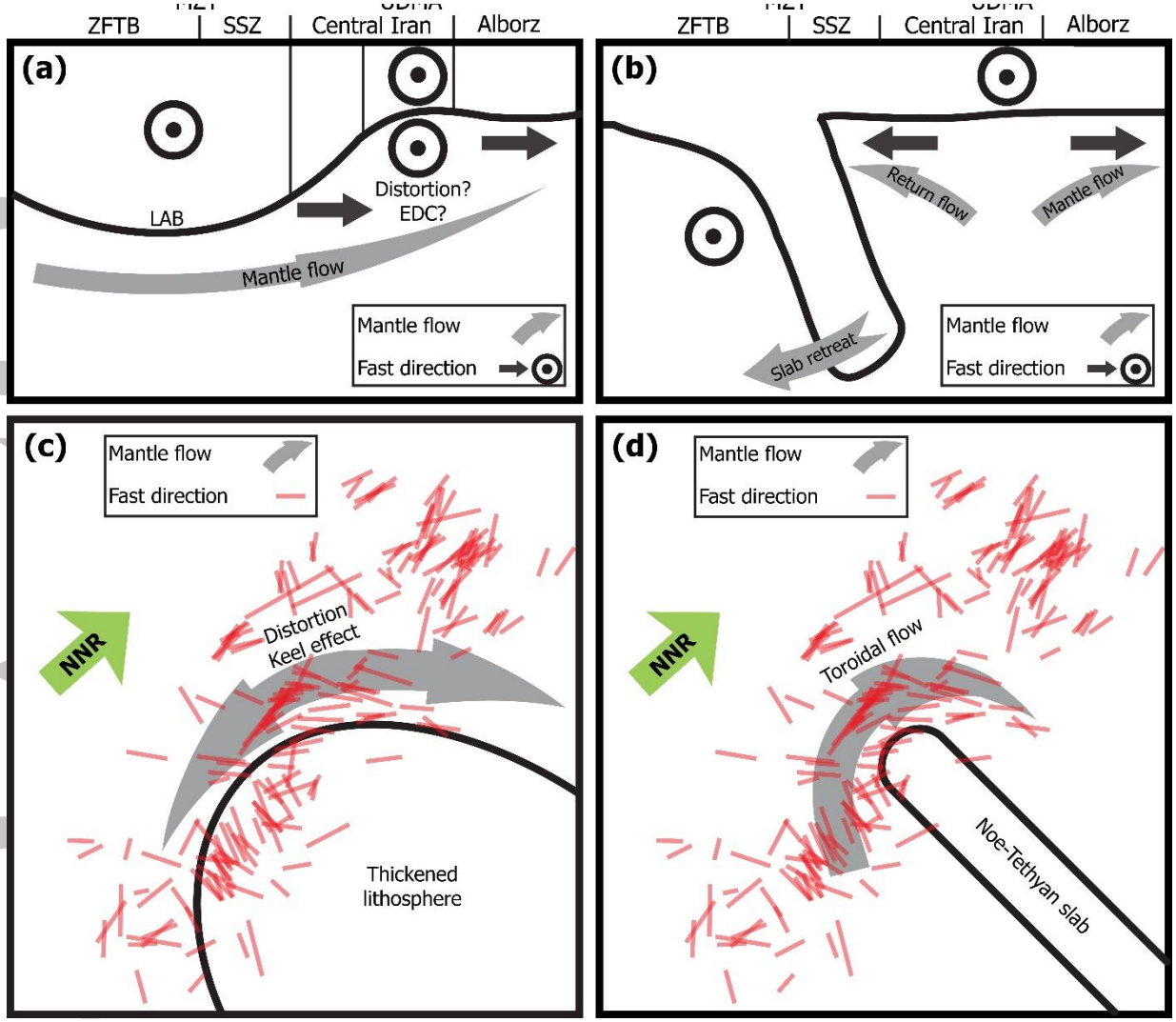

Figure 6. Schematic 2D sketch of the two main geodynamic scenarios explaining the observed shear wave splitting measurements in Arabia-Eurasia collision zone; (**a**) is the slab break-off scenario and (**b**) shows the subduction associated scenario. The approximate locations of the thickened Zagros lithosphere in the slab break-off scenario and the Neo-Tethyan slab in the subduction associated scenario, both at 150 km depth, are projected to the surface in (**c**) and (**d**), respectively. The individual splitting measurements at 150 km piercing depth are also shown by the transparent red bars. Abbreviations are defined as follows: ZFTB, Zagros Fold-and-Thrust Belt; MZT, Main Zagros Thrust; SSZ, Sanandaj-Sirjan Zone; UDMA, Urmieh-Dhokhtar Magmatic Arc; EDC, Edge-Driven Convection; NNR, No-Net-Rotation.

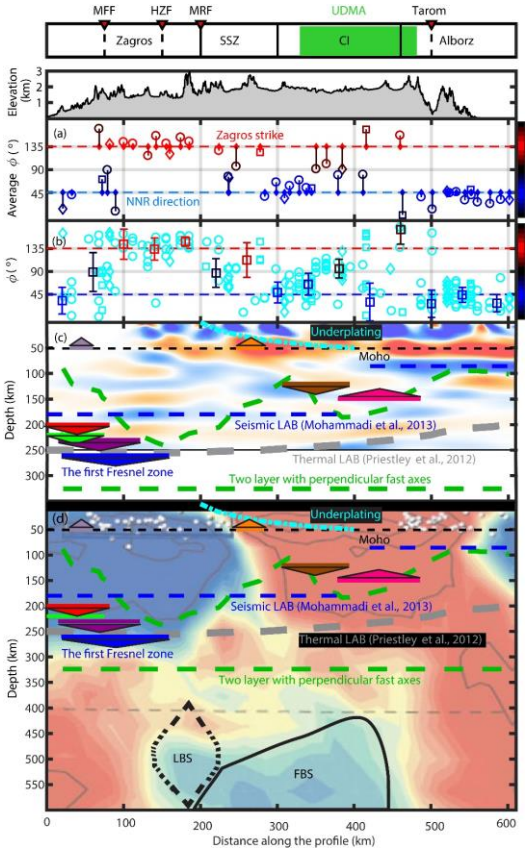

Figure 7. Two top rows and abbreviations are same as Figure 3. (**a**) The bidirectional circular average of fast-axis orientations (Equation1) at stations are projected on the middle profile. Average values at the eastern, middle and western profiles are shown by diamonds, circles, and squares, respectively. The Zagros strike and the absolute plate motion directions are also shown by colored dashed lines. The color of symbols varies based on the value of average fast-axis orientations and according to the color bar on the right. Blue and red symbols are parallel with the no-net-rotation (NNR) direction and Zagros strike, respectively, and the average values between them are represented by black color. Each fast value is connected to the corresponding fast orientation in the simplified two-layer model with perpendicular axes. (**b**) Individual measurements are projected on the middle profile and shown by cyan markers. Their bidirectional circular averages and standard deviations in 40 km bins are shown by error bars. Color of the binned averages and error bars are the same as the color of the markers in (**a**). Migrated S receiver functions along the western profile of Mohammadi et al. (2013) and the P wave vertical tomographic transect of Vergés et al. (2011) are shown as background in (**c**) and (**d**), respectively. LAB depth estimated by Mohammadi et al. (2013) (blue dashed line) and Priestley et al. (2012) (gray dashed line) as well as the lithospheric thickness predicted by two-layer anisotropy model with perpendicular fast-axes (undulating green dashed line) and depths estimate by first Fresnel zones are superimposed on the background in (**c**) and (**d**). The approximate locations of the first broken-off (FBS) and the last broken off (LBS) slabs are shown in (**d**).

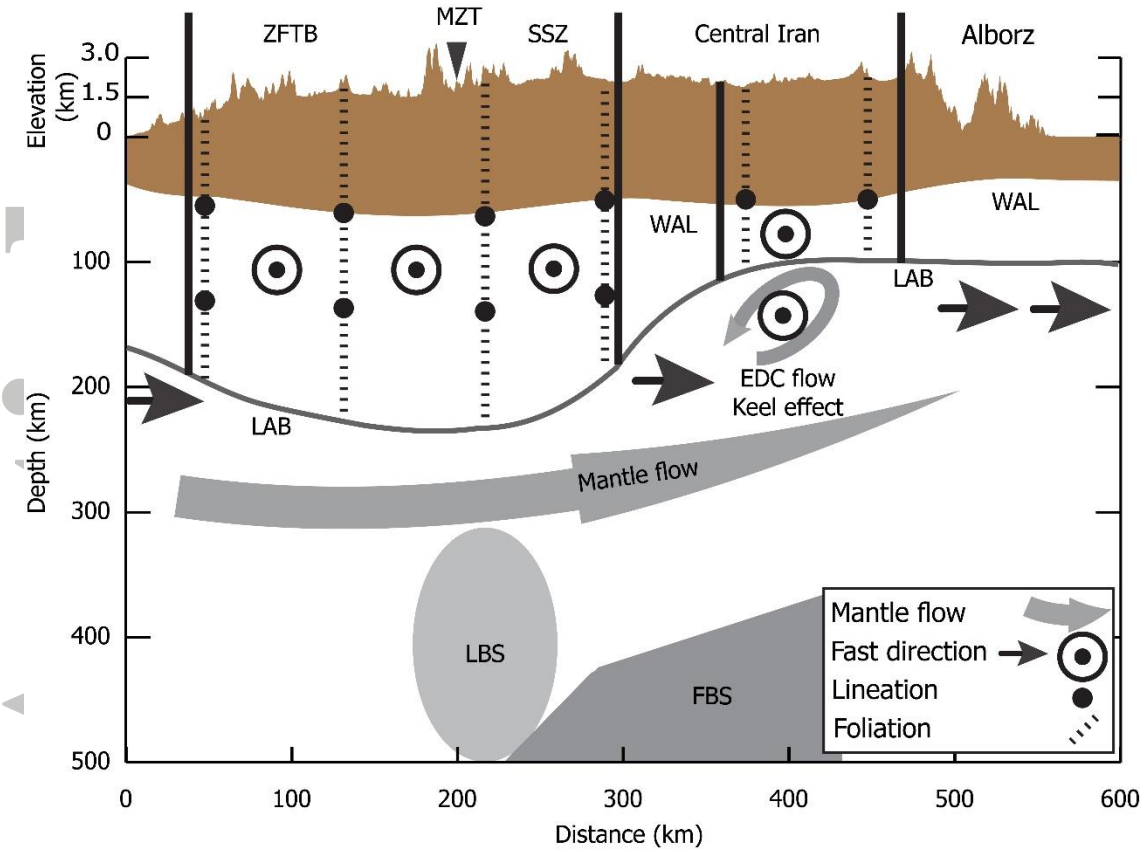

Figure 8. Our preferred 2D geodynamical model of the western Arabia-Eurasia collision zone beneath the middle profile of seismic stations analyzed in this study, crossing the western Zagros, central Iran and western Alborz. The crustal part is shown by brown area. The range-parallel fast-axis orientation in the Zagros Fold-and-Thrust Belt (ZFTB) and Sanandaj-Sirjan Zone (SSZ) originate from the lithosphere, whereas in central Iran, the Edge-Driven Convection (EDC) flow and the keel effect also contribute. The no-net-rotation (NNR) parallel fast orientations are associated with the asthenospheric flow field beneath the thin and/or weakly anisotropic lithosphere (WAL) inferred from Pn anisotropy. The approximate locations of the first broken-off (FBS) and the last broken-off (LBS) slabs are shown.

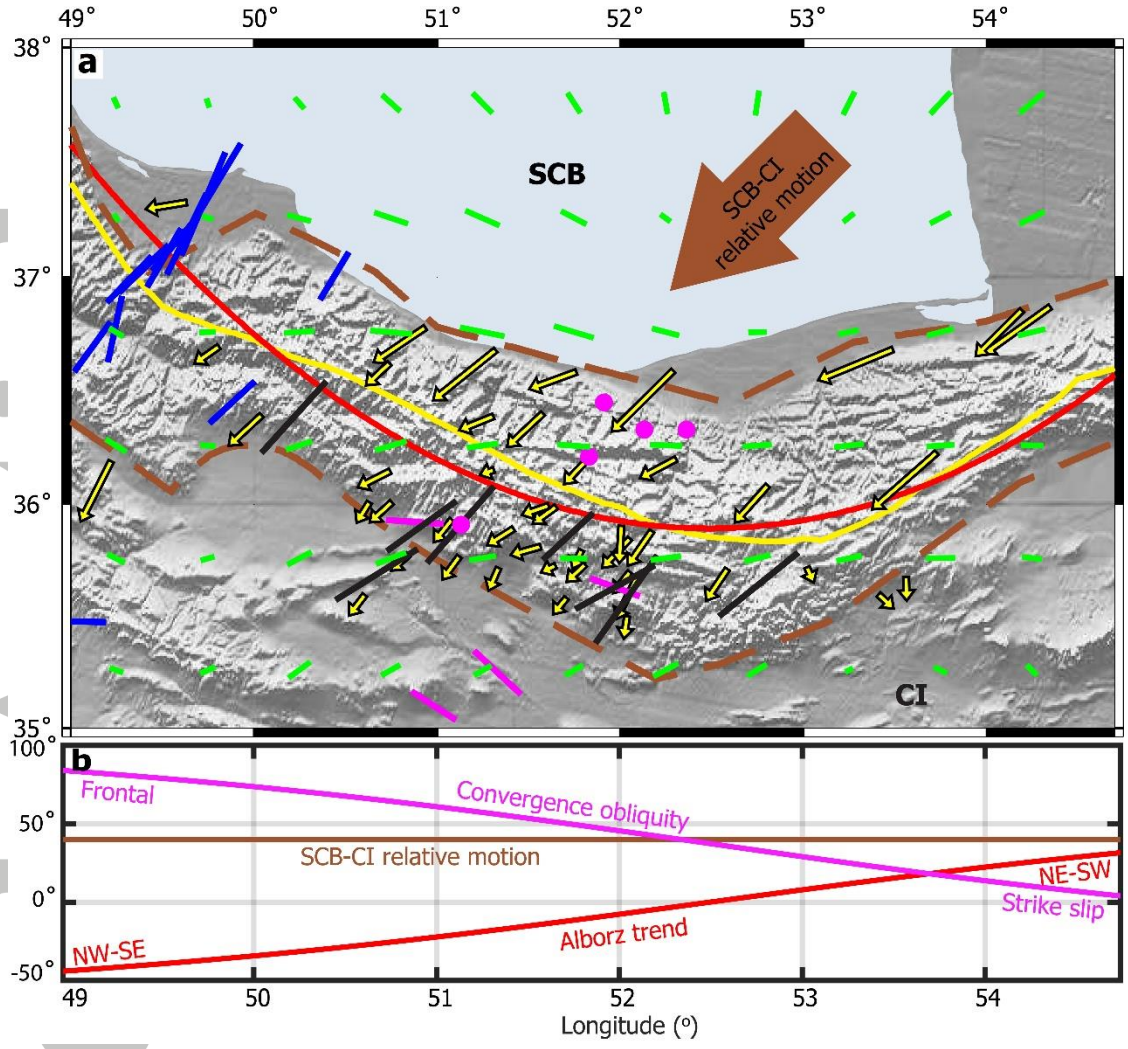

Figure 9. (**a**) GPS velocity vectors of Djamour et al. (2010) relative to central Iran are shown by yellow arrows. The borders of South Caspian Basin (SCB), Alborz and central Iran (CI) are marked by dashed brown lines (Shabanian et al., 2012) and the relative motion of SCB and central Iran is illustrated by thick brown arrow. Yellow line is the smoothed Alborz trend estimated from free-air gravity anomaly and red line shows a second order polynomial fitted to this trend. Blue, magenta and black markers are the splitting results of Sadeghi-Bagherabadi et al. (2018), Kaviani et al. (2009) and Sadidkhouy et al. (2008), respectively. Green bars illustrate the Pn anisotropy measurements (Lü et al., 2017). (**b**) The slope of the fitted second order polynomial to the Alborz range trend is plotted by red line. The average relative motion between SCB and CI is shown by brown line. Purple line shows the angle between SCB-CI relative motion and the Alborz trend. The convergence obliquity in western Alborz is frontal and it tends to be strike-slip to the east.

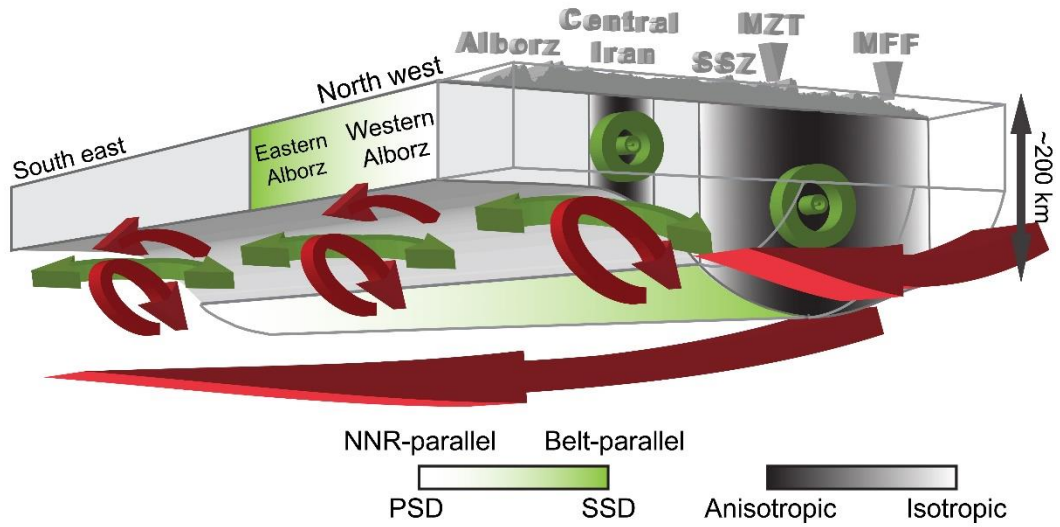

Figure 10. 3D geodynamical model of the Arabia-Eurasia collision zone. The no-net-rotation (NNR) parallel fast orientations, associated with the asthenospheric flow field are shown by red arrows and the green arrows show the range-parallel sublithospheric flow caused by Edge-Driven Convection (EDC) flow. The lithospheric range-parallel fast orientations in western Zagros and central Iran are shown by green markers. The gray shading in lithospheric section represents the amount of deformation and its associated anisotropy in lithosphere. The green shadings plotted at the base of the thickened Zagros lithosphere and along the Alborz lithospheric section show the variation in the style of lithospheric deformation along theses fold-and-thrust belts. The pattern of deformation in the western Zagros and eastern Alborz is simple shear-dominated (SSD) transpression that gradually changes to pure shear-dominated (PSD) transpression pattern towards central and eastern Zagros and western Alborz. This variation in the deformation style will coincide with the shift from the lithospheric belt-parallel fast-axes in the western Zagros to a NNR-parallel trend in the eastern Zagros. In Alborz, however, the plate motion parallel trend to the west changes to the non-belt-perpendicular pattern to the east.